SINTER-SWAGE PROCESSING OF AN Al-Si-Mg-Cu POWDER METALLURGY ALLOY

By

Margaret Wilson

Submitted in partial fulfilment of the requirements
for the degree of Master of Applied Science

at

Dalhousie University
Halifax, Nova Scotia
August 2021

Table of Contents

List of Tables

List of Figures

Abstract

The focus of this study was to develop a powder metallurgy (PM) equivalent to the versatile aluminum alloy 6013, for which a PM variant does not yet exist. This helps to broaden the scope of applications for PM. A secondary objective was to assess the mechanical response of the 6013 PM equivalent to hot deformation processing. To approximate extrusion, a laboratory-scale hot swaging process was used. Four PM equivalents to wrought alloy 6013 were explored. The presence of manganese and tin were varied across the four alloys. Alloys containing manganese were found to respond poorly in sintering trials, while tin had a varying effect on sintering response. However, all alloys were found to respond positively to swaging, achieving densities of >99% of theoretical. No defects were observed in any alloy system following swaging. Appropriate heat treatment parameters for the alloys were established for T6 and T8 heat treatments. To further explore the alloy equivalents, the mechanical properties of the alloys were assessed in three different processing sequences. These were sinter-T6, sinter-swage-T6, and sinter-swage-T8. The mechanical properties were compared to wrought. Tensile assessments found that samples processed through press-and-sinter performed poorly in comparison with wrought, particularly in terms of ductility. Samples that had experienced sinter-swage processing, were more comparable to wrought, exhibiting significant increases in tensile strength and ductility in both T6 and T8 conditions. In this same processing condition, T8 samples produced higher strengths, but lower ductility in comparison with samples in the T6 temper. Of the four alloy alternatives, PM6013-Sn performed best in all processing sequences during tensile testing and was selected for further examination. The fatigue behaviour of this alloys was assessed in the same processing conditions. The fatigue resistance of sinter-swage samples was found to be superlative to press-and-sinter samples. Overall, sinter-swage-T6 processing of PM6013-Sn produced the mechanical response more comparable to wrought alloy 6013. Some key areas of future work include characterizing PM6013-Sn further to allow for wrought comparison and a study of the response of PM6013-Sn to industrial hot forging.

List of Abbreviations Used

DSC – Differential Scanning Calorimetry

E – Young's Modulus

EDS – Electron Dispersive Spectroscopy

GP – Gunier-Preston

HRB – Rockwell Hardness Scale B

HRE – Rockwell Hardness Scale E

LPS – Liquid Phase Sintering

MMC – metal matrix composite

OAL – Overall Length or thickness

PM – Powder Metallurgy

R – Extrusion Ratio

SEM – Scanning Electron Microscope

UTS – Ultimate Tensile Strength

wt. % - weight percentage

σ_a – Fatigue Stress

Acknowledgements

The author would like to acknowledge the funding support provided by the Natural Sciences and Engineering Research Council of Canada (NSERC) through grant CRDPJ 486528 – 15.

I would like to thank Dr. Paul Bishop for the input and support he has provided throughout this program. Thanks, as well, to the other members of my examining committee, Dr. Paul Amyotte and Mr. Ian Donaldson, for their insights.

It has been a pleasure to work alongside my colleagues in the Net Shape Manufacturing Group, past and present, and the wider Mechanical Engineering Department. I would be remiss if I did not specially thank Randy Cooke, for his assistance and patience with my many (many) questions.

Throughout this program, I have benefited from the skills of technicians. I would particularly like to acknowledge the support of Patricia Scallion of the SEM, and Mark MacDonald and the machine shop team. Lauren Davis of Sexton Library provided much appreciated assistance at the eleventh hour.

Finally, a big ‘thank you’ to my family for their love and support throughout this process.

Chapter 1. Introduction

This thesis focuses on a research investigation carried out into a powder metallurgy (PM) alloy, combined with additional processing. The research had dual objectives. The first was to develop a PM alloy equivalent to wrought aluminum alloy 6013. The successful development of this alloy system would promote the broader use of the versatile 6xxx series of aluminum alloys in commercial PM applications. The second objective was to assess the response of sintered products to hot deformation, particularly extrusion through hot swaging. The affect of the additional processing on the mechanical properties of the alloy was of particular interest.

In meeting these objectives, this thesis consists of three major components. These are contextualizing background information, (Chapter 2), a paper discussing the research that was carried out (Chapter 3), and finally a global summary which also contains some recommendations for future work (Chapter 4).

Chapter 2. Background

2.1 Aluminum Powder Metallurgy

Powder Metallurgy (PM) is an advanced manufacturing technique that provides a different approach to metalworking and processing than traditional technologies. The classic PM process has three basic steps: powder production, powder compaction and powder sintering/consolidation. Through the use of PM techniques, a metal powder of known attributes is converted via the application of pressure and thermal processes, to a 'strong, precise, high performance shape'[1]. PM is valued particularly because of its ability to produce net or near-net shape products, which typically require minimal machining prior to entering service.

The essentials of PM - subjecting metallic powder particles to heat to achieve a consolidated final product – were understood by the ancient Egyptians[1]. As an industrial technology, however, PM is relatively 'young'[2],[3]. Experimentation in PM occurred throughout the nineteenth and twentieth centuries, but the industrial applicability of PM became more competitive in the 1970s, leading to its broader use. Since then, PM has developed repute as a versatile, dependable and economical method of manufacturing components in large volumes [3]. It has been used to produce both structural and functional components.

PM has substantial advantages over traditional manufacturing techniques, the most notable of which is ability to fabricate near-net shape products. Because PM processes do not utilize as high temperatures as casting methods, PM can be used to process some niche alloys and composites. It has also been observed that PM products produce comparable tensile properties to cast products[4]. However, PM processes are burdened with the requirement for high-value tooling. Hence, components must be produced by PM in large volumes to be economically viable. In addition, the maximum size product that can be fabricated through PM is also limited by constraints to the upper loads available in compaction and sizing presses.

Initially, industry focus was on the application of PM techniques to structural ferrous steels. In the modern PM industry, a more diverse selection of metals that may be utilized. PM is now regularly applied to stainless steels, aluminum, copper, titanium, and metal matrix composites. Aluminum and its alloys have been widely processed utilizing PM techniques for the automotive

industry. In North American passenger vehicles, for example, aluminum is the second most plentiful material in the car, second to steel components [2].

Aluminum is an appealing candidate for PM because it has an excellent combination of mechanical and physical properties including a high strength-to-weight ratio, good machinability, and corrosion resistance as well as excellent heat conductivity properties. In the automotive industry, aluminum alloys have been used to manufacture components for a range of applications including camshaft bearing caps, gears, thrust and retainer plates, and variable cam phasers [3]. These components are all produced at high volume and require strict dimensional tolerances.

2.1.1 Powder Production

Powder production is an important step in the conventional press-and-sinter PM process because powder characteristics, such as particle size and morphology are determined at this stage. These have a significant impact on the compaction and sintering response of the powder, which in turn affects the properties and performance of the completed PM component.

Aluminum powders are principally produced through gas atomization. In this fusion-based process powder particles are formed from molten metal, by creating a spray of droplets using a compressed gas as the atomizing medium [1], [5]. Atomization is popular because it can be easily applied to a range of alloys and provides control over melt purity and alloy chemistry[1].

Atomization may be done in either a horizontal or a vertical orientation. The vertical orientation is more commonly used, as it can produce wider range of powder particle sizes [6]. A schematic of a typical vertical gas atomizer is illustrated in Figure 1.

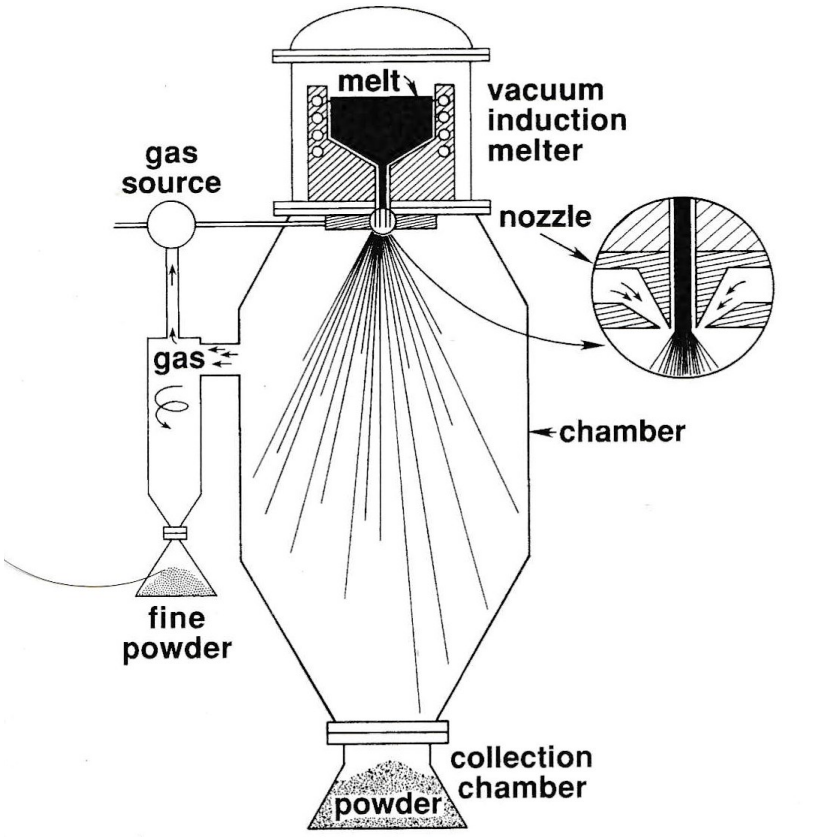

Figure 1: Schematic illustrating vertical gas atomization [1]

In vertical atomization, the metal or alloy of interest is melted in a crucible at the top of the apparatus via induction heating. The liquid metal then flows through an opening in the bottom of the crucible into the atomization die. Here, the molten stream then disintegrates into small droplets due to the rapid depressurization of the atomizing gas [7]. As the droplets travel downward through the chamber they solidify into discrete, solid particles that are collected at the bottom of the unit. Atomizing gas is then recirculated or exhausted directly to atmosphere. In both cases a cyclone or particulate filter trap is present in the exhaust line to trap fine particulates.

A variety of gases may be used for atomization including compressed air or inert gases such as helium, nitrogen, or argon. The choice of atomizing gas can impact powder morphology. For example, use of an inert gas yields spherical particles, while an irregular shape prevails when using air [5]. Inert gas atomization is sometimes preferable as it reduces the impurities present in the powder product, particularly oxide content. In aluminum powders, the thickness of the oxide

layer or film (Al_2O_3) is often dependent on the oxygen content of the atomizing gas[5]. More oxygen is present in compressed air atomization processes than in inert gas processes, hence a thinner oxide film forms when the latter is used. A thin oxide film is desirable in PM processes, as it typically promotes enhanced sintering. Inert gas atomized powders typically contain under 100 ppm oxygen, whereas air-based particulates can exhibit up to 3000 ppm oxygen[1], [4].

Atomization is a popular powder production technique because the powders it produces have characteristics that make them amenable to PM processing. Gas atomization imparts good flow, packing, and compressibility properties. Atomization parameters such as nozzle geometry, flow rate of gas, gas pressure, gas composition, flow rate of molten metal, and the temperature of the molten metal may be adjusted to control the size of particles obtained [1], [6]. Atomization is also popular because it can produce high volumes of elemental and alloyed powders [1].

2.1.2 Powder Compaction

In order for solid products to be created from aluminum powder, the particulate feedstock must be consolidated. This is accomplished in two steps: compaction and sintering. Die compaction is the most common method of initially consolidating aluminum powders. Here, the powder is loaded into rigid tooling comprising a die, punches, core rods, and other components. Then, sufficient uniaxial pressure is applied to form the powder into a coherent compact [1]. Once pressed, a compact is referred to as ‘green’, to differentiate from fully consolidated, sintered compacts. The fluid-like characteristics of powders mean that they respond positively to applied pressure over a range of stresses [7]. Uniaxial pressing is usually used in conjunction with aluminum powders, as they are relatively easy to compact [5]. This is carried out using a rigid die cavity and plunger system, constructed of a tool steel or a cemented carbide. Such materials are used for the die tooling to prolong the life of the system because of the abrasive nature of the metallic powders being processed. The pressing action may be accomplished using single, dual, or floating action presses. Uniaxial pressing allows for construction of complex parts using specialised die sets. The limiting factor of the pressing operation is the shape and size of the rigid die cavity[8].

Because most compaction tools are made from tool steels, they are prone to seizing and galling during the compaction of aluminum powders. As such, a lubricant powder is generally admixed

into the raw powder system of interest [5]. The lubricant also limits the accumulation of friction during interaction of the powder with the die walls and punches, thereby decreasing the magnitude of density gradients in the green compact [5]. This helps to avoid cracking, warping and other distortions of the compact during the sintering process[9]. Despite the addition of lubricants to powder blends, friction, particularly from the die wall, can never be fully mitigated. Lubricants used in combination with aluminum powders are commonly stearic acid-based waxes and compounds, and are typically added at concentrations of 0.5% to 1.5% by weight of the overall powder mixture[5].

Compaction is an important stage of the PM process because it instills the approximate shape of the intended final product while concurrently influencing the sintering response [10]. As indicated in Section 1.1.1, powder characteristics have a significant effect on compaction behaviour. In particular, powder compressibility and flowability are important to consider. These two related characteristics, affect the strength and density of the powder compact. The powder properties that contribute most directly to compressibility and flowability are apparent density and flowrate. Apparent density quantifies the bulk density of loose packed powder particles, while flowrate defines the displacement and interaction responses of powder particles to an external force, usually gravitational. These properties are important because they allow powder behaviour during subsequent processing steps to be predicted and controlled [7]. Powders with good flowability and compressibility properties result in the best properties and consistency in the final compacts [11].

The parameters of a compaction operation are dictated by the type of component being pressed. For example, the pressure exerted by the die and the speed of compaction are tailored to the powder and the shape of the compact. The pressure forces the deformation of powder particles to allow for improved packing density over that of the loose powder [10]. Particles undergo four key stages during compaction to form a green compact[5], [11].

1. Particle Rearrangement
2. Localized Plastic Deformation
3. Homogeneous Plastic Deformation
4. Bulk Compression

These phases are illustrated in Figure 2. The pressure at which each stage engages is powder specific.

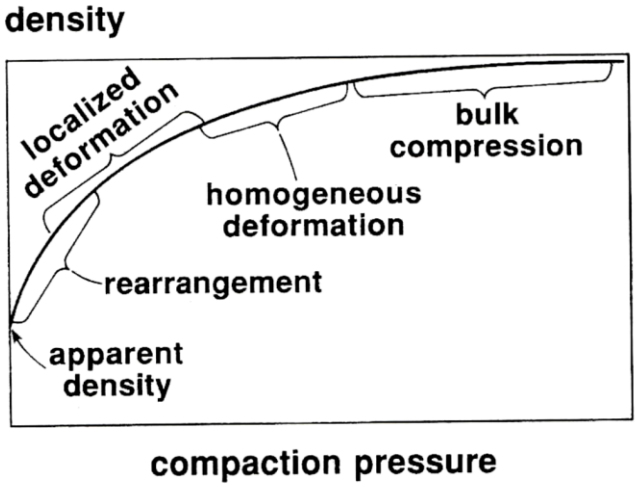

Figure 2: Graph showing engagement of the four stages of compaction [1]

In the particle rearrangement stage, powder particles shift and slide to become more densely packed. Particles also experience some elastic deformation at this stage. There is a substantial density increase in the compact during the rearrangement stage [11]. Once the particles have become closer packed, the second phase engages. In localised plastic deformation, particles are deformed such that inter-particle contact points expand. This occurs as particles deform and flatten under pressure[5], [11]. Homogeneous deformation then occurs as the pressure increases and the deformation becomes more uniform. This causes the plastic deformation behaviour to extend through the compact, as particles deform sufficiently to flow and fill inter-particle voids. Because voids are being filled during this stage of the process, particle centres come closer together. This means that there is a continued increase in density during this stage[11]. In the final stage of compaction, bulk compression, particles are all fully plastically deformed. Here, the compact behaves as a fully dense solid, undergoing uniform deformation throughout[11]. There is a small increase in density at this stage. The effect of compaction is illustrated in Figure 3.

Once the compaction cycle has been completed, the compacts are ejected from the die. When doing so, most will experience some elastic relaxation, or ‘spring back’. This can impact the

dimensions and density of the compact and may also lead to delamination if the compaction pressure was too high[11]. In industrial settings, compacts are typically pressed into the homogeneous deformation stage to facilitate process robustness[1].

Once pressed the compact has green properties which are dependent on the powder and compaction parameters [6]. Two of the most important characteristics are density and strength. A high green density is desirable because it generally results in an improved sintering response and final properties over a compact of low green density[10]. High green strength is desirable because it allows the compact to be handled with minimized propensity for chipping and/or cracking [1].

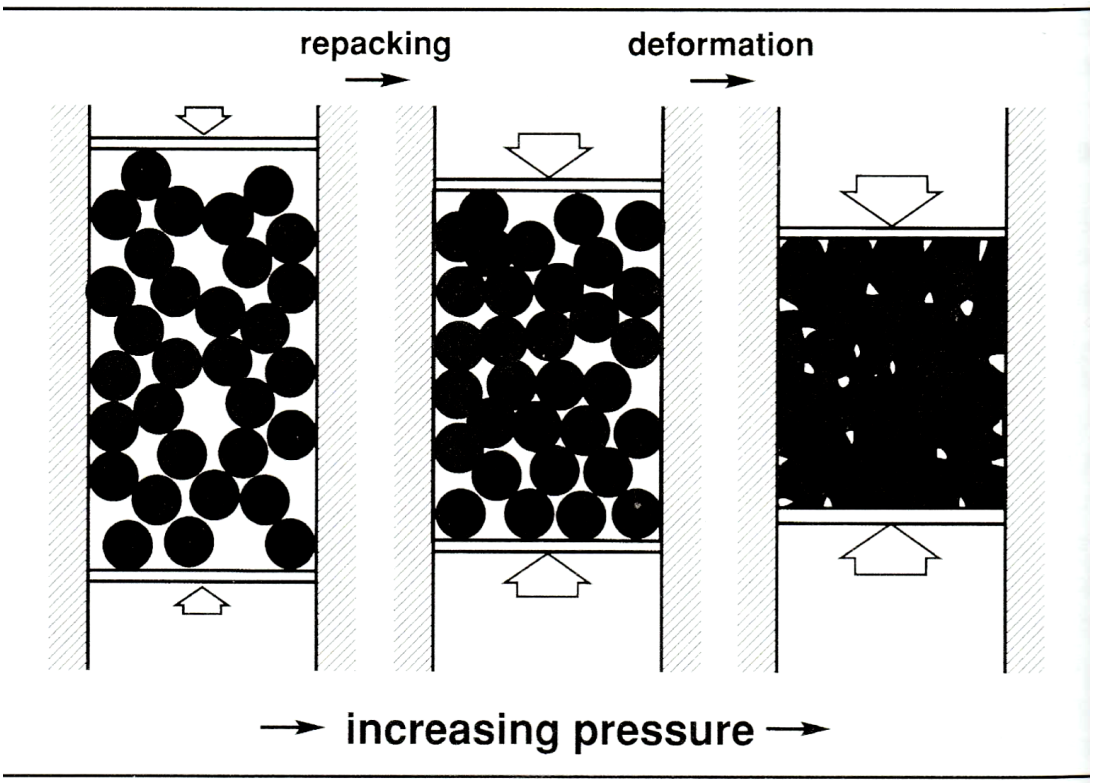

Figure 3: Schematic showing creation of powder compact[1]

Powder compaction has another use in aluminum PM processing because of the natural presence of the oxide layer, Al_2O_3 on the surface of aluminum powders. Usually between 50-150 Å in thickness, the Al_2O_3 oxide retards the sintering response of the powders, unless disrupted[5], [12]. Powder compaction helps to mechanically disrupt the oxide film, through the distortion of particles. The formation of contact points between particles causes the oxide film to rupture,

resulting in metal-to-metal contacts between particles, rather than oxide-to-oxide contacts. The former allows for the formation of localized cold welds between particles and aids sintering [4]. The importance of the disruption of the oxide layer will be discussed more fully in Section 1.1.3.

2.1.3 Sintering

Once the compaction process is completed, strength is developed in the shaped compact through the consolidation of particles. The most common method utilised for consolidation is sintering. Fundamentally, sintering is a thermal process, analogous to firing, that activates the bonding of particles to form a coherent, solid final product [5], [10]. It improves strength and determines many of the final physical properties of the component. The driving force for the sintering process is the decrease in total surface energy of the compact[5]. The bonding that occurs during sintering removes free surfaces, causes the growth of grain boundaries (low surface energy), and reduces the presence of porosity [5].

The success of the sintering process is assessed by dimensional and density changes over time. Successfully sintered products will usually exhibit shrinkage and densification. Shrinkage is the decrease of sintered compact dimensions as compared with the green compact. It must be carefully controlled in manufacturing to ensure that the product dimensions are correct and consistent. The degree of shrinkage that occurs may be predicted by ensuring controlled conditions within the sintering furnace. It is accounted for by oversizing the green compact [1]. Densification is an increase in the density of the sintered compact as compared with the green compact. Both shrinkage and densification result from the changes in the size, structure and volume of pores present in the green compact because of the bonding that occurs in the sintering process.

Sintering is carried out under highly controlled conditions in a furnace [12]. Parameters such as dew point, oxygen content, atmosphere type, and temperature in the furnace may be controlled to ensure a successful sinter. Sintering temperature, in particular, is specific to the material and chemistry of the compact [10]. As sintering has a significant impact on the mechanical and physical properties of PM components, time-temperature sintering profiles must be optimised.

Sintering profiles consist of three key stages. First, a de-lubrication period is used to remove the lubricant added for compaction. This occurs at a temperature of approximately 350°C. Compacts are then heated to the desired sintering temperature and isothermally held for a prescribed period of time, dependent on compact chemistry. Sintering is done at temperatures below the solidus of the compact in the case of solid-state sintering. However, the process can also involve a liquid phase. In most aluminum systems, the liquid phase sintering (LPS) mechanism is employed. Both concepts are outlined in the sections that follow.

2.1.3.1 Solid State Sintering

Solid state sintering occurs between solid particles in a compact. There is no liquid phase present in solid state sintering.

There are six mass transport and diffusion mechanisms (Figure 4) that are key to solid state sintering. There are three surface transport mechanisms:

1. Evaporation-Condensation: vapor flows into the bonding region between two grains, the 'neck'. Higher pressure in this area causes the vapor to condense in the neck.
2. Surface Diffusion: vacancies in the metal lattice diffuse from the neck to convex regions at the particle surface. A countercurrent of atoms diffuses to the neck, helping to bond the particles.
3. Volume Diffusion: a surface diffusion mechanism engages again here, except that the diffusion of vacancies and atoms occurs through the volume of the grain to the surface.

and three bulk transport mechanisms:

1. Plastic Flow: in regions local to the concave neck surface, particles deform and flow to help grow the neck and promote densification.
2. Grain Boundary Diffusion: because of highly energetic nature of grains boundaries, atoms and vacancies diffuse along them at a faster rate, helping to fill pores and build the neck region.
3. Volume Diffusion: the same volume diffusion mechanism outlined above engages, except that the diffusing atom originates in the particle bulk, rather than from the surface.

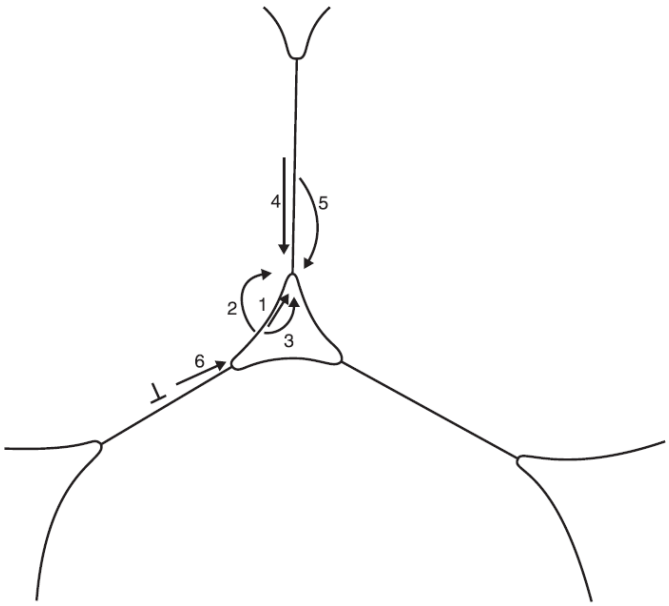

Figure 4: Image illustrating the 6 types of mass transport in solid state sintering; (1)Surface Diffusion; (2) Evaporation-Condensation; (3)Volume Diffusion(bulk); (4)Grain Boundary Diffusion; (5)Volume Diffusion(bulk); (6)Plastic Flow[5]

Visually, the three key stages of sintering are the Initial, Intermediate, and Final. The characteristic appearance of each is illustrated in Figure 5. The stages of sintering that engage are dependent on the condition of the green compact when sintering begins. In compacts where particles are highly flattened and stressed, the initial stage of sintering may not be observable. In compacts consisting of less deformed particles in point contact, all three stages of sintering will be observably present [10]. Note also that there is no clear distinction between the phases of sintering [10]. Each phase has characteristic events, but there is not a distinct 'trigger' for either onset or conclusion of any phase.

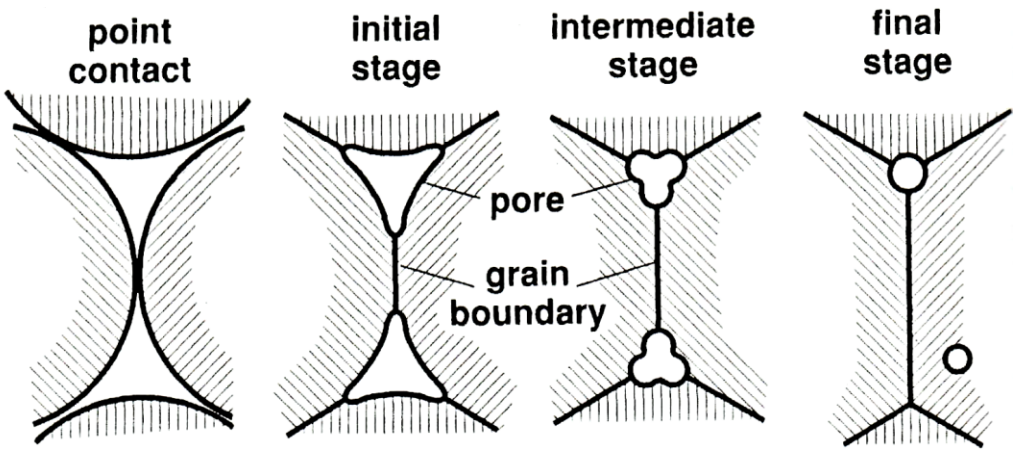

Figure 5: Illustration of the stages of sintering[10]

Initial stage sintering occurs during the heating process. The initial bonding between particles occurs in this stage. Having been compacted, there is already a weak cohesion between particles. This is consolidated with the rapid growth of a metallurgical interparticle bond, called a neck. Necks grow independently of their neighbours [10]. Very little densification results from this stage, but the curvature gradient of the particles is substantially reduced [10]. Surface transport mechanisms are dominant in this phase.

The initial stage of sintering is only active for early neck growth. Neck growth continues and necks stabilize in the intermediate stage of sintering. The intermediate stage is important for densification, as the focus shifts away from neck growth to the elimination of pores in the compact. Pores may be considered as large collections of vacancies in the 'lattice' structure of the compact. So, pore elimination is dependent on the movement of vacancies. For this to occur, bulk transport mechanisms must engage, with mass flow originating from the particle bulk rather than particle surfaces as in initial stage sintering [10]. Surface transport mechanisms are still active in intermediate stage sintering, evident in the changing structure of pores throughout the phase. As the intermediate stage progresses, the size and volume of pores decreases. Pores become less interconnected and develop a smoother structure. Grain growth occurs late in the intermediate stage as pore structure shifts and grains become larger than the initial particles[10].

The final stage of sintering is more gradual in comparison to the initial and intermediate stages. It is characterized by further grain growth and development. Pores continue to be eliminated in this phase, though more slowly than in the intermediate stage. Pores become spherical and closed, forming the final structure of the component [10].

2.1.3.2 Liquid Phase Sintering

LPS is commonly used in the sintering of alloy mixtures of powders or pre-alloyed powders. It is applied to components with multiple phases that melt over a range of temperatures above the solidus line of the alloy phase diagram, so that the liquid and solid coexist for at least a portion of the sintering cycle [5], [13], [14].The versatility and adaptability of LPS means that it is one of the dominant sintering approaches in commercial applications [13].

A key feature of LPS is the development of capillary forces as a result of the presence of the liquid phase. Such forces develop at the solid and liquid interfaces, pulling grains together and intensifying densification in a briefer period of time [5], [13]. Caution is warranted when employing LPS: increased amounts of distortion can occur and brittle phases can precipitate along grain boundaries to the detriment of mechanical properties [5].

There are different types of LPS, categorized by the liquid phase that forms. Persistent LPS is the more common, where the solid phase is soluble in the liquid phase at a given sintering temperature[13]. This is not the case in the less common transient LPS where the liquid phase dissolves into the solid phase gradually over time[13].

To successfully progress with either type of LPS, some basic conditions must be met. First, the liquid phase must wet the solid. Wetting describes the interactions between solid, liquid and vapour phases that exist in the compact and defines the ability of a liquid to maintain contact with a solid surface. A system may be wetting or non-wetting. A wetting system is one in which the solid-liquid surface energy is less than that of the solid-vapour surface energy, resulting in a contact angle of less than 90°. Non-wetting systems result in a contact angle between the liquid and solid surfaces greater than 90°[5]. Good wetting properties are important in both types of LPS because it increases the contact area and strength of the capillary forces. A wetting system also shows improved penetration of grain boundaries by the liquid phase, which enhances compact densification [5].

The second condition for successful LPS is that the alloying addition that ultimately forms the liquid phase should have low solubility in the base, or solid, phase. This ensures adequate liquid volume and segregation at the interparticle boundaries where it is needed to enable shrinkage and

densification [5], [12]. Should the alloying addition have a high solubility in the base swelling and unsuccessful sintering may result.

The third condition is that the solid, base phase must have high solubility and high diffusivity in the liquid phase. This ensures high mass transport rates, resulting in rapid sintering and densification. It is best for the liquid to be completely miscible as this helps to ensure rapid mass transport and that no intermediate solid metallic phases form during the sintering process[5], [12].

The final condition is that the alloying addition should have a lower melting point than the base metal to allow for the spontaneous formation of a liquid phase and the progression of LPS. An alloying addition that shares a low melting point eutectic with the base may also be used, but the sintering process is less straightforward[12].

There are three key phases in the LPS process that follow the formation of the liquid phase. They are:

1) Primary Rearrangement
2) Penetration and Fragmentation
3) Secondary Rearrangement/Solution Reprecipitation

The overall process is illustrated in Figure 6. In the primary rearrangement stage, particles in contact with the liquid phase move relative to one another to achieve improved packing efficiency. Rearrangement is driven by interparticle pressure – a combination of capillary forces and liquid-vapour surface tension – and varies with wetting angle. The packing density achieved in this phase is dependent largely on efficient contact between the solid and liquid, so a homogeneous distribution of the liquid phase is particularly important [5]. During this phase, the particles become tightly packed, and pores become less interconnected. Primary rearrangement stops when the particles are as tightly packed as possible without additional deformation.

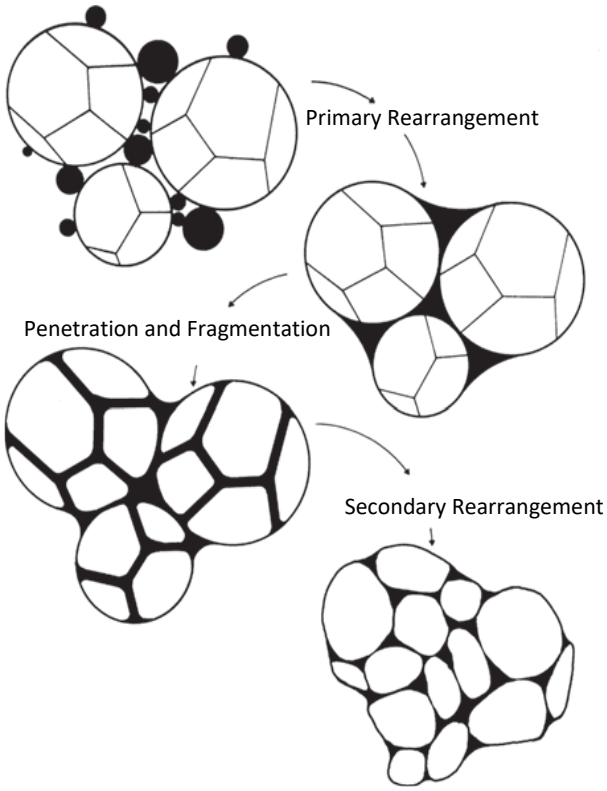

Figure 6: Figure illustrating the phases of LPS [5]

During the penetration and fragmentation stage, the liquid phase penetrates the grain boundaries of the rearranged particles. This splits up and fragments the particles into smaller pieces. Swelling in the compact may occur here before further repacking and densification in the final phase. The penetration of the particle grains effectively induces the stage of secondary rearrangement wherein the compact densifies further[13]. Now, densification is achieved through the combination of grain growth and grain shape accommodation that culminates in pore elimination. Ostwald Ripening – the dissolution of small grains followed by reprecipitation on larger, existing grain structures - is one of the mechanisms of grain growth[5]. Shape accommodation occurs through contact flattening. Mass transport through diffusion during the LPS process results in the flattening of grains at solid-liquid interfaces. This decreases the overall distance between particles and leads to densification in the compact[5].

2.1.3.3 Sintering of Aluminum

Sintering of aluminum alloys is achieved through LPS under an atmosphere of high purity nitrogen that is dry and low in oxygen content. Nitrogen has emerged as the preferred gas as it results in the best sintering response and is an economical choice for industrial production. According to Schaffer et al, nitrogen enhances sintering through the preferential formation of aluminum nitride over Al_2O_3 thereby decreasing the thickness of the oxide layer [4]. The presence of aluminum nitride leads to an increased rate of shrinkage during LPS and, concomitantly, improved densification. Careful control of the dew point and temperature during sintering can aid in the development of well-sintered products. Although optimum dew point is dependent on the alloy and powder, an approximate guide is a dew point of -60ºC or lower. Temperature should be controlled such that a margin of $\pm$3ºC from the intended sintering temperature is maintained [4], [5].

The liquid phase itself results from the incorporation of alloying additions which either have a lower melting point than aluminum or react in-situ to form low melting point eutectics. As noted in Section1.1.2, the oxide skin on the surface of aluminum powder particles makes them challenging to sinter and must be disrupted for successful sintering [5], [12]. Oxide layers can be problematic in the sintering of other types of powders (e.g., ferrous) as well, but these can usually be eliminated by sintering in a reducing atmosphere. In the case of aluminum however, this is not possible because the oxide is thermodynamically stable under the practical range of atmospheres and sintering temperatures that can be employed. Solutions are chemistry-based, emphasizing additions of elemental magnesium and tin.

Magnesium acts as both a reducing agent to disrupt the oxide film and as an oxygen getter to further lower the presence of this impurity in the sintering atmosphere. Magnesium also helps to encourage the development of aluminum nitride particles, further reducing the impact of the oxide film. Further, electron microscopy has demonstrated the presence of spinel crystallites in the sintering of aluminum-magnesium alloys. It is posited that their development leads to the creation of shear stresses in the oxide film, ultimately resulting in its break-up [12]. Through all these mechanisms, the presence of magnesium allows for sinter bonding to develop fully between particles. Typically, only a minor concentration of magnesium is required to facilitate

improved sintering, although the amount is dependent on the size of the aluminum powders and the net amount of surface area present. The mechanisms by which magnesium aids in the sintering of aluminum engage at approximately 500ºC [5].

Tin behaves differently, as it acts as a catalyst in the LPS of aluminum powder systems [4], [5]. Specifically, it helps to decrease the surface tension of the liquid phase so as to improve its wetting behaviour. Research has suggested that elements favourable to the formation of liquid phases during LPS tend to gather at the liquid-vapour interface. By altering the surface tension, the wetting behaviour of these components is enhanced through improved liquid spreading. However, the effect of tin must be monitored between alloy systems as its impact is not universally positive. For example, it is beneficial in Al-Mg-Si systems, but in others it can decrease the capillary pressure during the LPS, negatively affecting the sinter quality. Tin can also influence the formation of aluminum nitride if it is present in a sufficient concentration. Small amounts of tin can be effective for process control during LPS of aluminum powders under nitrogen atmosphere [4].

2.1.4 Commercial Alloy Systems

There are a number of commercial aluminum alloy systems available in PM including conventional and composite materials [1]. However, in comparison to wrought aluminum alloys, the portfolio of commercial PM alloys is limited. As this factor has stifled industry uptake of PM, a common feature of aluminum PM research is the development of new alloys for industrial use [4],[15]. PM alloy equivalents have been produced by a number of organizations including GKN Powder Metallurgy, Ampal, Toyal America and Ecka Granules [16][15]. In most instances, developments have targeted formulations based on commonly used wrought alloys, yet the compositions are not necessarily identical. For example, aluminum PM alloys may contain additions of tin, to aid in the sintering performance as discussed in Section 1.1.3.3. The main driving force behind alloy development is to obtain PM alloys that can compete with wrought and cast counterparts in terms of mechanical and physical properties.

A common thread in aluminum PM alloy development has been research into materials that offer advantageous combinations of strength, thermal stability, and/or wear resistance. Some key examples include:

- PM equivalents in the Al-Mg-Si system which were found to be competitive with wrought alloys 6061 and 6063 [17].
- The alloy denoted Alumix-231 which demonstrates similar properties to wrought alloys in the 2xxx series [18].
- The development of a PM equivalent to alloy wrought 2618, which demonstrates good thermal stability [19].
- Wrought alloy 2324, one of the strongest alloys in the 2xxx alloy series, has also been successfully replicated. The PM equivalent to the wrought material demonstrated considerable gains in tensile strength properties, but lowered ductility in the T1 heat treatment condition when compared with the wrought alloy [15].
- The 7xxx series of wrought alloys has also been of interest, particularly alloy 7075, because of the high strength properties observed in the wrought alloy. Examples of this alloy series in use include Alumix-431D which demonstrates a comparable mechanical performance to wrought alloy 7075[15], [16].

2.2 6xxx Series Alloys

Naturally plentiful, aluminum is one of the most widely used metals today ranging in applications from industrial machinery and aircraft to household foil. One of the reasons for its broad popularity lies in its versatility. Aluminum can perform well across a broad range of physical and mechanical requirements. It is a comparatively light-weight metal, with a density of ~2.7 g/cm^3[20]. A high-strength-to-weight ratio makes aluminum particularly attractive for structural and engine-based applications. Aluminum also has strong corrosion resistance, making it usable in freshwater, seawater, soil, foods and some chemical media[21]. It is also responsive to a range of processing techniques.

The relatively low strength of un-alloyed aluminum limits its commercial applicability, so it is often alloyed to improve its mechanical properties[20]. To support a specific set of properties for a given application, aluminum alloys may be tailored to meet those requirements. Aluminum alloys are designed both to undergo specific processing conditions and to perform to specific conditions in a service environment [12]. For example, some alloys are intentionally designed to exhibit lower strength to permit greater ease of extrusion processing.

Systems for both wrought and castable aluminum alloys exist. The designation ‘wrought’ indicates that the alloys are available primarily in the form of worked products. Working processes produce a wrought structure from a cast ingot[22]. As discussed in Section 1.1.4 wrought alloys are often used as the basis for the development of novel alloys to be used in an advanced manufacturing application, such as powder metallurgy. Castable alloys do not feature as often in the design of powder metallurgy alloys. Accordingly, this paper will focus on the wrought alloy systems, as they are most relevant to the development of powder metallurgy alloy equivalents.

The four-digit Aluminum Association system of nomenclature for wrought alloys is commonly used to differentiate alloys. The system divides alloys into groups, based on the primary alloying addition(s). The groups are indicated by the first of four digits as follows:

- 1xxx indicating un-alloyed aluminum.
- 2xxx indicating a primary alloying addition of copper.

- 3xxx indicating a primary alloying addition of manganese.
- 4xxx indicating a primary alloying addition of silicon.
- 5xxx indicating a primary alloying addition of magnesium.
- 6xxx indicating primary alloying additions of silicon and magnesium.
- 7xxx indicating a primary alloying addition of zinc.
- 8xxx indicating a primary alloying addition of lithium.

[20], [23]. In this nomenclature, the second digit indicates the alloy modification or variant. For example, in the 2xxx series, the designation 20xx indicates that the alloy is unmodified from its original design. The third and fourth digits have no special role in the naming and serve only to differentiate between alloy compositions.

2.2.1 Overview of wrought 6xxx alloy systems

The 6xxx series is a popular aluminum alloy system. This series of alloys combines intermediate strength and mechanical properties with good formability, weldability, and machinability. The 6xxx series also offers good corrosion resistance [20]. Strengthening is accomplished through solute precipitation making the 6xxx series one of the foremost systems of heat-treatable aluminum alloys [22], [23]. Though not as strong as other heat-treatable systems, like the 2xxx and 7xxx series alloys, the unique combination of properties has fostered widespread use.

6xxx series alloys contain primary alloying additions of magnesium and silicon. Generally, additions of magnesium range from 0.6-1.2% by weight (hereafter wt. %) and of silicon range from 0.4 -1.5wt. %. Wrought 6xxx series alloys may also contain small additions of copper, chromium, and manganese[20], [23].

Magnesium and silicon are usually present in sufficient quantities to produce the magnesium silicide phase (Mg_2Si). This hard, metastable intermetallic phase gives 6xxx series alloys their heat-treatable properties. Alloys containing 0.6 wt. % Mg_2Si demonstrate strong precipitation hardening behaviour (see Section 1.1.2.2 for further discussion) [23]. While magnesium and silicon are usually present nominally in quantities consistent with the formation of Mg_2Si, silicon may be present in amounts excess to this requirement. Excess silicon provides an increase in the strength of the alloy, but a corresponding decrease in corrosion resistance. Excess magnesium

has an entirely negative effect, as it reduces the solid solubility of Mg_2Si [20]. Manganese and chromium are included because they have been shown to provide both strengthening and grain-size control. Manganese, in particular, assists in strengthening and improving mechanical properties, through the development of the intermetallic dispersoid Al_6Mn [24]. Copper may also be present in 6xxx series alloys as a strengthening agent. Copper provides additional strengthening through control of precipitate growth, ensuring the dispersion of fine precipitates throughout the aluminum matrix. However, if added in quantities larger than 0.5wt. %, copper may negatively impact corrosion resistance[22], [23].

6xxx series alloys may be divided into three groups. This is not a formal nomenclature system; rather it delineates alloy groups according to usage and alloying additions. In the first group, the total addition of magnesium and silicon does not exceed 1.5 wt.%, with very little excess silicon. These alloys are often used in extrusion applications. An example of an alloy in this group is 6063. The second group contains 1.5 wt.% or more of combined magnesium and silicon, with little excess silicon. Other alloy additions that may also be present are copper, manganese and chromium. Alloys in this group, such as 6061, are typically used for structural applications. In the third group, the amount of silicon is in excess of that required for the formation of Mg_2Si. The overall amount of magnesium and silicon may be 1.5 wt.% or more. Additions of manganese and chromium are particularly common in this group as they can assist in controlling the recrystallization of silicon during heat treatments. The addition of less common elements, such as lead and bismuth, may also be seen in this series. Examples of alloys in this series include 6010, 6013 and 6262[20].

The chemistries of several common 6xxx series alloys are shown in Table 1. This illustrates the range of chemical compositions included in the 6xxx alloys. A representative alloy from each ‘group’ is also present to illustrate the differences in the chemistries.

Table 1: Alloy chemistries for a range of 6xxx series alloys [20], [23].

Alloy	Group	Alloying Element Content (by wt. %)						
		Al	Mg	Si	Mn	Cr	Cu	Other
6010	3	Balance	1.0	0.8	0.5	-	0.38	-
6013	3	Balance	1.0	0.8	0.5	-	0.9	-
6061	2	Balance	1.0	0.6	-	0.2	0.27	-
6063	1	Balance	0.7	0.4	-	-	-	-
6262	3	Balance	1.0	0.6	-	0.09	0.27	0.55 (Pb); 0.55(Bi)

Mechanically 6xxx series alloys usually achieve an ultimate tensile strength (UTS) on the order of 300 MPa with ductility of around 10-15% elongation. In contrast, other age-hardening alloy systems, such as the 7xxx series, have a UTS on the order of 500MPa, with similar ductility. Values for UTS, yield strength and elongation properties for a range of 6xxx alloys are illustrated in Table 2. All data are for materials in a T6 heat treatment condition.

Table 2: Typical tensile properties for a range of 6xxx series alloys in T6 condition [20], [25]

Alloy	UTS (MPa)	Yield Strength (MPa)	Elongation in 50mm (%)
6010	386	372	11
6013	399	368	11
6061	310	275	12
6063	241	214	12
6262	310	276	17

The properties of the 6xxx series alloys lend themselves to a wide variety of applications. For example, alloy 6061 is one of the most widely used aluminum alloys in industry. It's intermediate strength and formability properties make it an excellent general-purpose alloy, particularly in structural applications [23]. Other alloys are more tailored to specific process requirements. For example, alloy 6013 is valued for its amenable response to welding and other hot processing technologies [23].

Other applications include structural and flooring components for transit and marine vehicles, heavy-duty land and marine structures, wire/rod products, rivets, furniture, architectural components, tubing, pipelines, forgings and extruded products[23].

2.2.2 Heat treatment of Al-Mg-Si alloy systems

6xxx series alloys can be heat treated through a range of processing sequences, the specifics of which are indicated by the "Tx" temper designation [20]. Typical tempers for this family of alloys include T4, T6 and T8. All of these comprise the basic steps of solution heat treatment (i.e., "solutionizing"), water quenching, and aging. The T4 temper consists of a solution heat treatment, followed by a quench to room temperature and aging at room temperature to improve and stabilize mechanical properties. The T4 temper strengthens the alloy, while maintaining reasonable formability after heat treatment. The T6 temper involves a solution heat treatment, followed by water quenching to room temperature and artificial aging process wherein the alloy is held at a moderate temperature (i.e., ~150 to 190ºC). The yield strength and UTS of T6 treated products are generally superior to those found in the T4 state, yet they are usually unsuitable for post-heat treatment forming operations. Finally, the T8 temper designation applies to products which have been solution heat treated, quenched, and then cold worked prior to an artificial aging process. Cold working is usually done in the form of flattening, straightening, or stretching. This can substantially improve hardness, yield strength and UTS but at the expense of ductility, which decreases [20],[26].

Each of the three components of the thermal treatment, and the respective temperatures utilized therein, influence the microstructure of the alloy. Pertinent data on microstructural development can be gathered from the Al-Mg_2Si phase diagram (Figure 7).

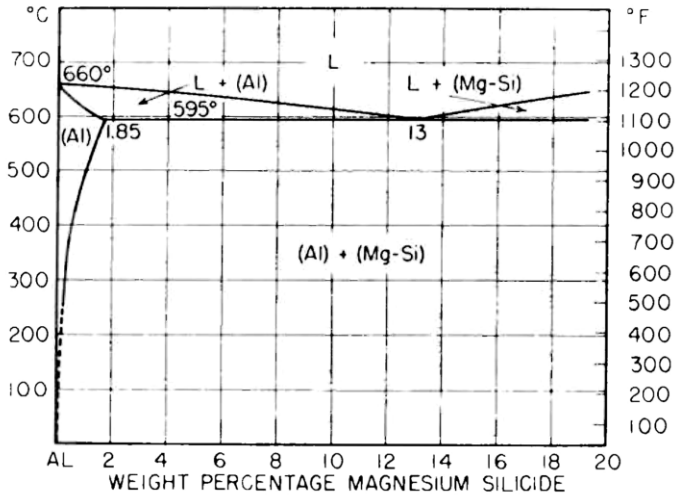

Figure 7: Al-Mg_2Si phase diagram[23]

The solution heat treatment phase involves heating the alloy to a temperature above the solvus line of the phase diagram and holding there for a period of time sufficient to form a single phase. Figure 8 shows a detailed view of this area on the Al-Mg_2Si diagram. The single phase formed is a super saturated solid solution. Quenching 'locks in' this structure, allowing it to be retained at ambient temperature. In order to preserve the structure, quenching should be as rapid as possible [26].

Once quenched, structures are aged. Aging is achieved by reheating the alloy to a temperature below the solvus and below the Gunier-Preston (GP) miscibility gap. The aging process allows for the precipitation of a fine intermetallic phase throughout the material. As a result, aged microstructures are often complex. The intermetallic precipitates are usually composed of the main alloying additions in the alloy, in the case of 6xxx series alloys, Mg_2Si. As a result, precipitates tend to be solute-rich, while the rest of the structure is solute-weak. Precipitates form as solute atoms diffuse and nucleate. Initially, this occurs in a localized manner with the first precipitates usually forming at grain boundaries, or near dislocations. Cold working helps to strengthen the material as it forms more dislocations, thus providing more nucleation sites for precipitates. The distribution of precipitates broadens as the aging process progresses. The rate of precipitate growth is diffusion controlled [26].

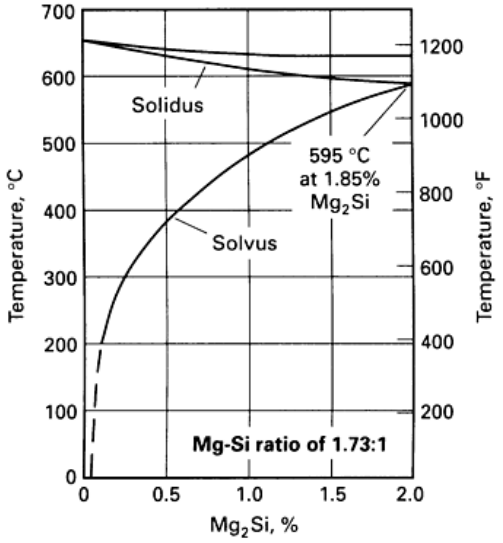

Figure 8: Section of the Al-Mg_2Si phase diagram [26]

The general precipitation sequence that occurs during aging of Al-Mg-Si alloys is as follows:

$$\text{Supersaturated solid solution} \rightarrow \text{GP Zones} \rightarrow \beta' (Mg_2Si) \rightarrow \beta (Mg_2Si)$$

As clusters of solute rich atoms develop, solute-rich GP zones form first. It is thought that the GP zones have a needle or acicular morphology and are oriented in the <001> direction in the matrix [23]. These evolve into needle shaped β' precipitates that are semi-coherent and, eventually, into the equilibrium phase β that is also needle-shaped, but larger and fully incoherent. The nature the Mg_2Si precipitate formed in the finished product is highly dependent on the aging time and temperature employed. If the artificial aging time is excessively long, coarse precipitates of β will be the dominant structure. Similarly, if the aging temperature used is too hot, the amount of solute available for precipitate formation decreases as does the concentration of precipitates present. Both scenarios result in decreased mechanical properties and are to be avoided. Generally, a combination of parameters that coincides with a high density of β' precipitates coincides with peak strength. The combination of parameters also varies with the alloy and desired temper. To illustrate this, parameters that combine to produce an optimal microstructure, and in turn, maximum mechanical properties for the T6 condition for a range of alloys are shown in Table 3.

Table 3: Heat treatment parameters for T6 temper for various 6xxx alloys [20], [26]

Alloy	**Solutionizing Temperature (ºC)**	**Solutionizing Time (hours)**	**Aging Temperature (ºC)**	**Aging Time (hours)**
6010	565	2	175	1
6013	570	2	190	4
6061	530	2	175	8
6063	530	2	175	8
6262	540	2	170	12

Tempers have a varying effect on the mechanical properties of alloys. This effect is illustrated in Table 4. For a given temper, the optimal properties in 6xxx series alloys are achieved through rapid quenching and the immediate start of aging processes after quenching[26]. Properties that are optimized using this treatment include strength parameters and corrosion resistance.

Table 4: Table showing the effect of tempering on the tensile properties of various 6xxx series alloys[20],[23], [25]

Alloy and Temper Designation	UTS (MPa)	Yield Strength (MPa)	Elongation in 50mm (%)
6010-T4	296	186	23
6010-T6	386	372	11
6013-T4	341	198	23
6013-T6	399	368	11
6061-T4	241	145	22
6061-T6	310	275	12
6061-T8	379	358	15
6063-T4	172	90	22
6063-T6	241	214	12
6063-T8	255	241	9
6262-T6	310	276	17

2.3 Extrusion Processing

2.3.1 Fundamentals

This section provides an overview of the fundamental concepts of extrusion processing with particular reference to the extrusion of aluminum alloys. Aluminum alloys are amongst the most commonly extruded metals in terms of both the number of products extruded and product value [27]. Most commercially available aluminum alloys are amenable to extrusion processing, mainly because of their physical metallurgical properties [28]. The face-centred cubic structure of aluminum with twelve slip systems and high stacking fault energy combine to give aluminum alloys good workability, making them "particularly suited for the extrusion of products very close to the finished shape and with attractive properties"[27].

2.3.1.1 General Extrusion Processes

Extrusion is a compressive forming technology which has applications in a range of manufacturing industries, including food, plastics, and metallic products. It is a popular manufacturing technique because it may be used to fabricate a finished or near-finished shaped product in a one step process. In the metalworking industry, extrusion is mainly used to produce bar, wire, and tube forms [27]. Complex shapes may also be produced, such as the heat sink shown in Figure 9 [29]. Extrusion is done when a billet, usually a solid square or circular block of material, is forced through a shaped die by applied pressure. Billet geometries are determined by the desired extrusion and the type of press being used. Extrusion products are straight and have a constant cross-section and a longer length than the starting billet [28]. There are few remaining tensile stresses in the extrusion product, allowing for a good finish and decreased requirement for secondary machining or heat treatment[27].

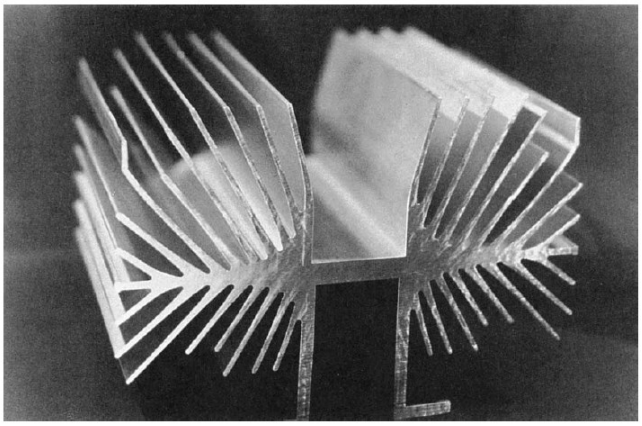

Figure 9: Image showing complex heat sink extrusion product[29]

There are variations in the way extrusion may be carried out. The billet may be passed through the die in either direct (forward) or indirect (backward) extrusion. These are illustrated in Figure 10a and Figure 10b, respectively. In both cases, the extrusion pressure is delivered by component 4 as shown on the diagram. The tooling used in extrusion processing is examined more closely in Section1.1.3.2.

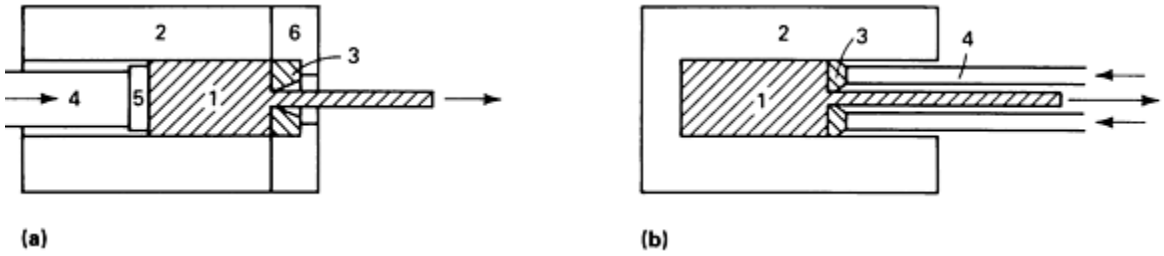

Figure 10: Basic methods of extrusion. (a) Direct (b) Indirect. 1, billet; 2, container; 3, die; 4, stem; 5, dummy block; 6, die holder [28].

Direct extrusion is done when the billet is forced by the stem through the die which is held in the container. In this case there is relative movement between the billet and the container. By contrast, in indirect extrusion the die is held in a stationary position by the stem and the billet is held in a container. The stem applies pressure to the stationary billet and the material is forced through the die. There is no relative movement between the billet and container[27], [29]. All

extrusion processes may be done in either the horizontal or vertical orientation, depending on the equipment being used.

Extrusion may be completed as a hot or cold process. In the former, the billet and the tooling are heated to an elevated temperature prior to the start of the process; typically, one that is slightly above the recrystallization temperature of the material of interest[27]. Cold extrusion is done when both the billet and equipment are at room temperature at the start of the extrusion process. These processes may be completed with or without lubrication. If used, lubrication is often achieved using graphite or glass-based lubricants for hot extrusion, and grease lubricants for cold extrusions [28].

Another approach to extrusion is hydrostatic extrusion. In this method, the billet is sealed in and surrounded by a pressurized fluid which allows the billet to pass through the die. Hydrostatic extrusion is typically used to extrude brittle materials which are not amenable to standard extrusion processing as the friction between the billet and the container is substantially lower in this method than in the other extrusion technologies[27].

The extent of extrusion is quantified by the dimensionless extrusion ratio, R, given in equation (1). The ratio quantifies the deformation that the billet undergoes in the extrusion process. R is usually defined as the ratio of the starting area, A_0, to the final area, A_f, but may also be obtained through length ratios.

$$R = \frac{A_0}{A_f} \tag{1}$$

Large scale deformations occur in extrusion processes as a result of the development of a state of compressive stress in the billet. For extrusion to be most successful (i.e., to result in a product with no cracking or defects), the material undergoing extrusion must have a low flow stress. Friction between the billet and the container and between the billet and the die acutely influences material flow[28]. The type of metal flow that engages during extrusion processes is also critical

to the success of the extrusion process. There are four key types, designated as “Flow Patterns”: S, A, B, and C. These are illustrated in Figure 11.

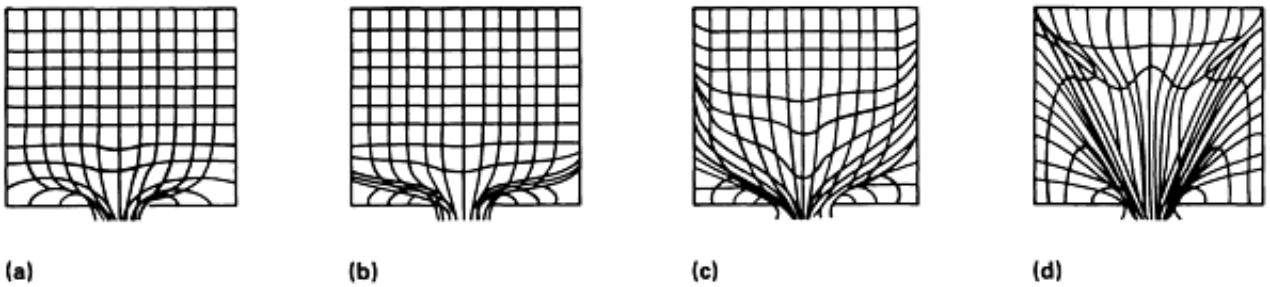

Figure 11: Images showing the common types of flow patterns encountered during extrusion; (a) S; (b) A; (c) B; (d) C [28].

2.3.1.2 Extrusion of Aluminum Alloys

Aluminum alloys are most commonly extruded using hot direct extrusion without lubrication [27]. The ‘hot’ temperature to which the billet is preheated varies depending on the aluminum alloy being processed, but is usually between 350-500ºC [27].

The selection of the preheat temperature of the billet is a complex decision since the actual temperature can change throughout the extrusion process as a result of heat from deformation and friction, as well as heat flow through the extrusion tooling itself, including the die and container [27]. Significant operating temperatures can develop on the working surfaces of the extrusion tooling [27]. The temperature can be controlled through heating the container to a different temperature from the billet, as the container is the most important heat sink of the extrusion tooling [27]. The temperature difference between the billet and container is limited to 50K which prevents the metal sticking to the sides of the container [27]. Whilst, the parameters of the extrusion process can also help to control the temperature of the extrusion, these factors are often competing. For example, to minimize the temperature of the extrusion, a high extrusion speed and a low extrusion pressure are desirable. But high extrusion speeds are achieved in combination with high extrusion pressures. Hence, the operating parameters selected are often a compromise between the two. The alloy being processed, and the quality requirements of the extruded product are also used to help determine the temperature range for the extrusion[27].

It is important to control the temperature of extrusions as the heating from friction and deformation that occurs during the process has an impact on the thermal history of the extrusion product [27]. For example, a typical heat-treatable aluminum alloy experiences a temperature profile during a hot extrusion process as shown in Figure 12.

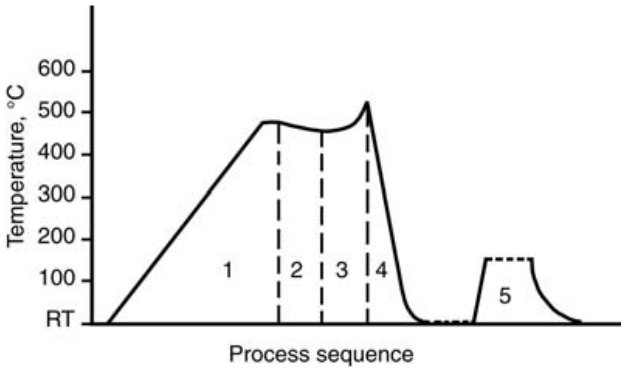

Figure 12: Graph showing process temperature profile experienced by typical heat-treatable aluminum alloy. 1) Billet heating; 2) transfer billet to extrusion press; 3) extrusion (effectively solutionizing); 4) section cooling; 5) age-hardening[27]

Aluminum alloys may be categorised by the ease with which they can be extruded. For example, 1xxx series aluminum alloys are categorised as easy-to-extrude, whereas 6xxx series alloys are moderately-difficult-to-extrude and 7xxx series alloys are difficult-to-extrude [27]. A range of factors are responsible for the extrusion behaviour of aluminum alloys, including the extrusion temperature range, friction across the tooling and the flow stress variation. The flow stresses and the pattern are dependent on the composition of the alloy and the extrusion process employed. In direct hot non-lubricated extrusion, the extrusion conditions under which most aluminum alloys are processed, Flow Pattern B is most likely to occur [27], [28]. A detailed view of Flow Pattern B is shown in Figure 13 for the case of a simple die opening, such as a square or circular geometry. For a more complex die opening, such as a channel or tube/mandrel, the same basic zones are present, but in a different, more complex arrangement.

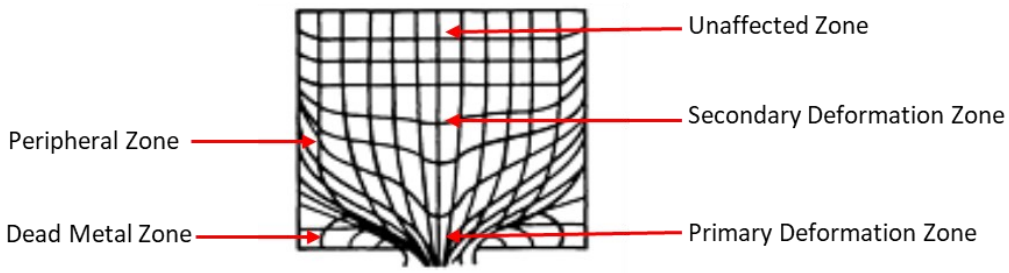

Figure 13: Labelled schematic of Flow Pattern B [28]

In this flow pattern, material flows by internal shear[28]. The deformation zone in Flow Pattern B encompasses a larger billet area than other flow patterns[27]. A dead metal zone, where no metal flow occurs, develops on either side in front of the die opening. Friction inhibits the flow of the metal close to the container walls, while inner portions of the material flow forward through the die. As a result, the surface of the extruded product is formed from the interior of the billet, as it shears along the stationary dead metal zone. The conical primary deformation zone is bounded by the dead metal zone and feeds into the die opening. The peripheral zone develops at the sides of the container, as shearing engages because of friction between the walls and the billet. In this zone, the deformation is up to 60 times larger than the plastic deformation at the core [27]. A secondary deformation zone occurs in the centre of the billet. It develops from the combined effects of shear and friction forces at the edges of the billet in the peripheral zone. Further back from the die opening, the billet core will remain unaffected and undeformed[27]. Deformation continues to occur as the extrusion process progresses and the billet core gets closer to the die opening.

Although many aluminum alloys respond favourably to extrusion processing, defects can form in the finished products. These include centre cracking, piping, and surface cracking (Figure 14). Others include uneven colour, surface roughness, poor material bonding, blisters, flaking, and a coarsened microstructure [27]. These defects can result in subsequent mechanical or corrosion damage to extruded components. Defects arise from inappropriate billet structure for the die, poor material flow, and/or incorrect extrusion temperature[27]. Defects can also arise if errors are made in the subsequent heat treatment or handling of extrusions.

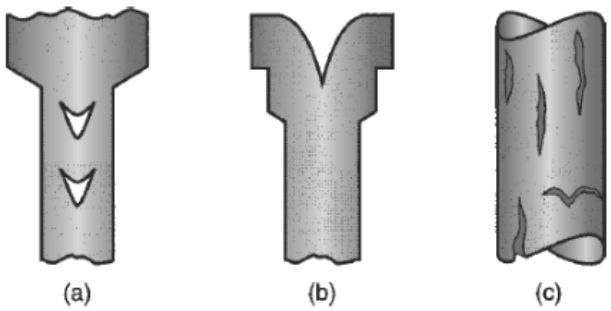

Figure 14: Images showing common extrusion defects (a)centre cracking; (b) piping; (c) surface cracking[29]

2.3.2 Commercial Technologies

Modern commercial extrusion operations take place in sophisticated organizations. They include a range of operational equipment and systems such as billet stores, billet heating, extrusion presses, handling equipment, cooling systems, saws and shears, heat treatment equipment, and packing lines. Data collection and quality management systems are also included to monitor production and ensure a consistent output [27].

Equipment and technologies vary with extrusion type. The most important direct extrusion presses are designed for the production of bar and hollow sections of aluminum alloys [27]. Direct extrusion presses are the focus of this section because they are used to process aluminum alloys. Direct extrusion presses of various kinds account for approximately 95% of industrial extrusion presses [27].

The commercialized direct extrusion press was introduced in the 1970s [27]. The key components of the press are shown in Figure 15 and remain representative of modern extrusion operations. The principal features of interest are:

1) The container in which the billet is held.
2) The extrusion die through which the billet is pressed.
3) The extrusion stem which applies pressure to the billet, to force it into the container and through the die.

4) The dummy block located between the extrusion stem and the billet. The block provides a ‘cushion’ between the softened alloy and the stem and helps to transmit force uniformly. It is commonly fixed in place during aluminum alloy extrusions.

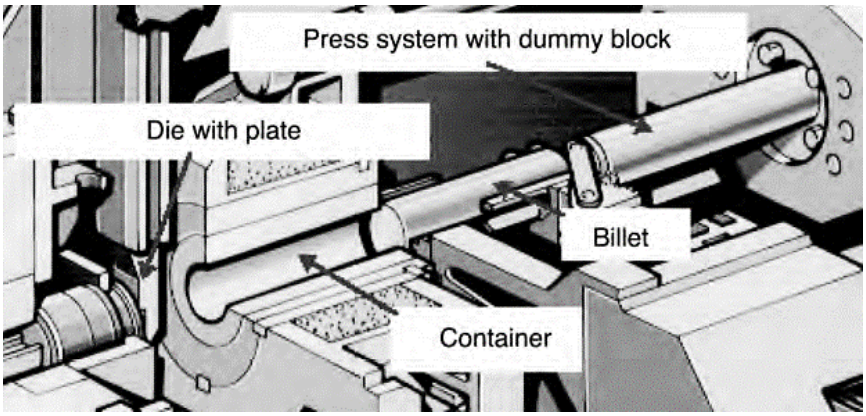

Figure 15: Image showing direct extrusion tooling[27]

Extrusion presses all have the same functional components, which are tailored to support specific applications. Apart from the die, the components listed above are not variable. Presses are made unique by the variation, addition, or removal of features and components. These may include the extrusion load, the press frame, the drive system, and the extrusion die.

The extrusion load is the defining parameter for equipment selection. The standard range of available extrusion loads in presses is between 5 – 125 MN[27]. Mid-size presses, with load capacities between 20-35MN, are those most commonly used commercially [27]. Careful selection of extrusion load is particularly important for presses which will be used in direct extrusion processes without lubrication. Here, the friction and shear forces can be up to 60% of the total extrusion load. If these frictional effects are not accounted for the extrusion process may be unsuccessful[27].

The press frame is an important component and contains all the press components and subassemblies [27]. Key features of a direct extrusion press subassembly include:

1) Main cylinder
2) Platen
3) Columns
4) Bed Plate

The design of the press frame must take into account the extrusion load, container and tool changing, and the requirement for some manipulation of these components during billet loading[27]. One of the most important characteristics of the press frame is its elastic behaviour during operation, as this influences the accuracy of guiding and support for the extrusion as it passes through the die[27]. A stiff frame will help to ensure that the extrusion does not twist as it is fabricated[27]. In direct extrusion, frame stiffness is usually accomplished through use of prestressed frames. These have low press extension, low deflection of assembly supports, and a short decompression time[27].

The drive system controls the speed of the extrusion process in commercial presses. Hence, it allows the speed of the process to be held constant or to be varied during a single extrusion cycle. Drive systems may be either water hydraulics, oil hydraulics, or electrical. In modern presses, oil hydraulics are the most common approach utilized. The components of oil hydraulic systems are less expensive than either electrical or water hydraulic driven systems and require fewer seals.

Extrusion dies are responsible for determining the shape of the extruded product. It is, therefore, important that the die be of a precise shape and maintain that shape when enduring the extrusion conditions. Die construction is done through a combination of CAD and CNC machining. The conditions under which extrusion is conducted mean that extrusion dies are exposed to high thermal and mechanical stresses. These include high thermal stresses where the tooling is in contact with the heated extrusion billet and in areas with high friction and/or shear forces. The speed of the extrusion cycle is also a factor in the wear of the die. Fast extrusion cycles effectively result in continuous loading, whereas slow extrusion cycles impose creep loading on the die. To handle these harsh conditions, dies are usually constructed from hot working tool steels.

The die can also be used to optimize the flow of material through the aperture. In aluminum alloys, material flow may be controlled through altering the lengths of die bearings. These are illustrated in Figure 16. As aluminum has a high affinity for iron, a thin layer of extruded aluminum material can develop on the die opening after numerous extrusions. This layer may be up to several micrometers thick. This causes poor surface roughness of extruded products.

Similarly, two main types of tool wear have been observed. Adhesive wear mainly occurs in the shape-forming aperture and can have a significant effect on the surface finish of the extrusion. Similarly, abrasive wear of the die leads to shape and dimensional inaccuracies in the extrusion product. Die maintenance is important to prevent and mitigate layer development and tool wear. Nitriding of the dies has been shown to be a useful treatment for the prevention of tool wear and the build-up of material on the die [27].

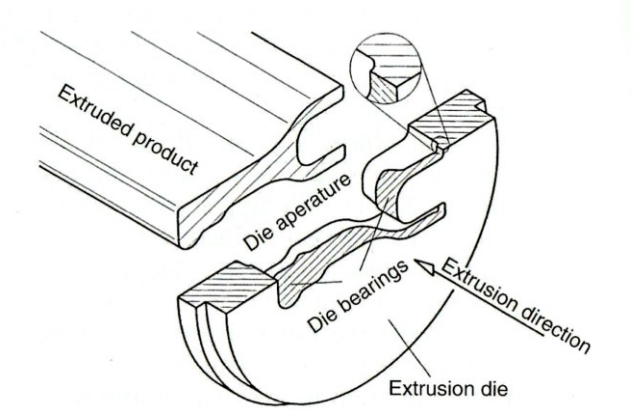

Figure 16: Schematic showing die bearings [27]

The most common direct extrusion press used today, the prestressed four-column press with a standard stroke, emphasises high volume output of product. The standard stroke consists of the container length, the designated clearance, and the billet length. The operation sequence for a direct extrusion press consists of the following steps:

1) Loading. The billet is brought into the press and placed between the stem and the container. The stem moves in the working direction.
2) Extrusion. This phase occurs from the initiation of the extrusion process (upsetting) until the predetermined discard length is reached. No further pressure is applied.
3) Clearing. The extrusion is separated from the discard length. Both are removed from the press. The press is returned to starting position.
4) Tool maintenance and preparation for future operations.

These phases are illustrated in Figure 17, for direct hot extrusion without lubrication.

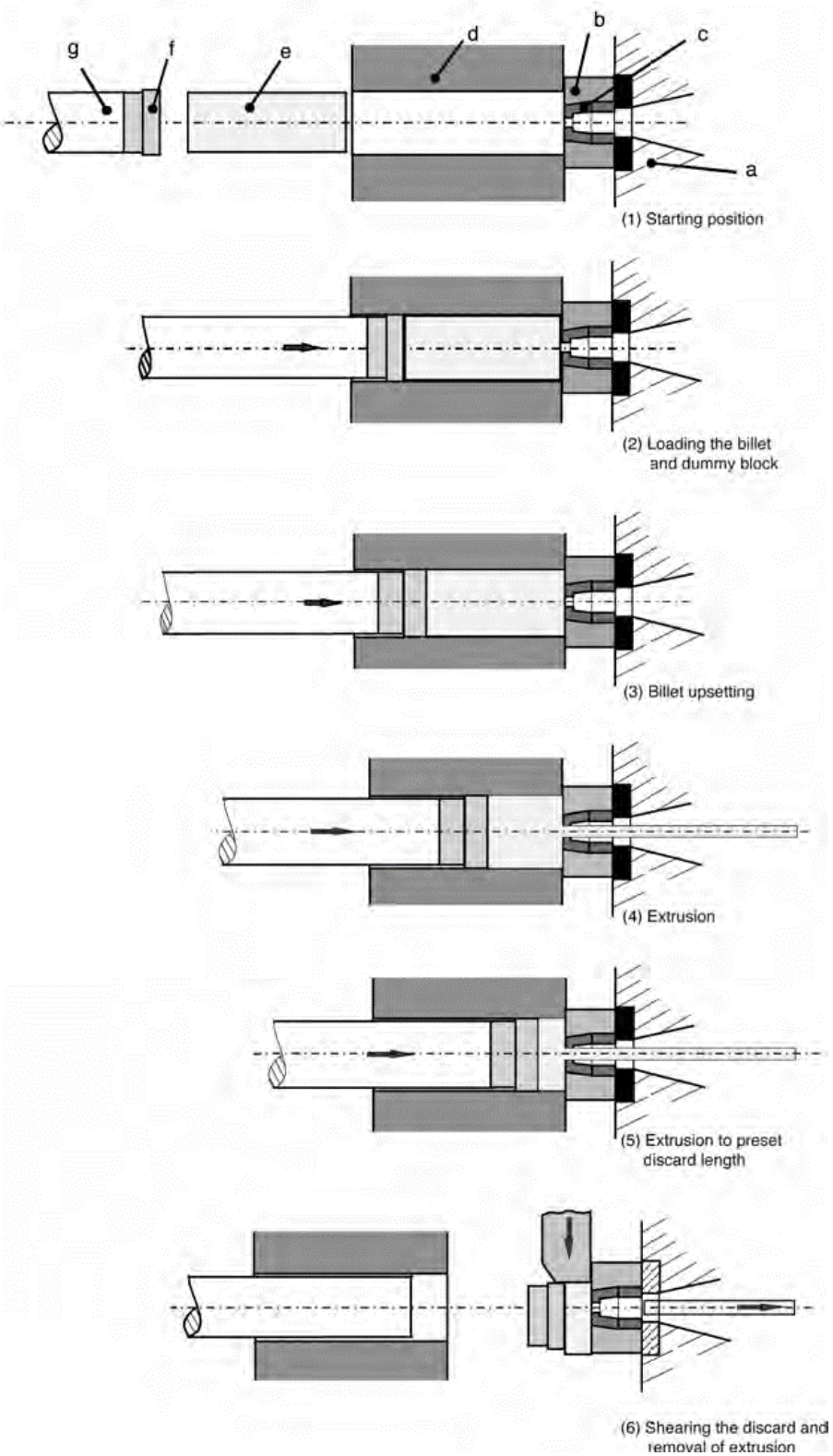

Figure 17: Schematic illustrating the basic process phases of hot direct extrusion without lubrication; where (a)platen; (b) die holder; (c) die; (d) container; (e) billet; (f) dummy block; (g) extrusion stem[27]

In recent years, new types of presses have been introduced. Short stroke presses are the current state of the art machines. The short stroke, at approximately 60% of a standard stroke, allows for greater control and accuracy of the extrusion than a standard stroke [27]. These presses are used for specialized extrusion tasks. They are more expensive than standard stoke presses because they have a more complex billet loading system, resulting in more equipment to maintain and slower production speeds. Front loading presses are also becoming more popular – as opposed to presses where billet loading is between the die and the container. In front loading presses, the alignment of billet with the die and stem centrelines are more reproducible. This allows for more consistent quality control of extrusion products. However, the billet requirements for front-loading presses are more stringent than for side-loading presses, so front-loading presses are not as popularly used.

Additional equipment may also be required in a commercial extrusion operation. The equipment required varies with the type of extrusion being produced, and the type of extrusion operation being carried out. For example, furnaces may be included to carry out billet heating, cooling tables may be present to cool a recently finished extrusion or handling systems may be used to manage completed extrusions. Many plants also include process control systems to manage the productivity of the plant and maintain the desired output of product along with product quality.

Extrusion may also be simulated in the laboratory setting. One method of simulation is rotary swaging. Swaging is a metalworking process that involves the reduction of the cross-sectional area by elongating the workpiece[30]. This effect is shown in Figure 18. The shape of the workpiece changes through metal flow, which can be multi-directional during the operation. Swaging is accomplished incrementally[30], through the use of multiple dies and repeated blows, as opposed to the use of a single die and continuous pressure in extrusion.

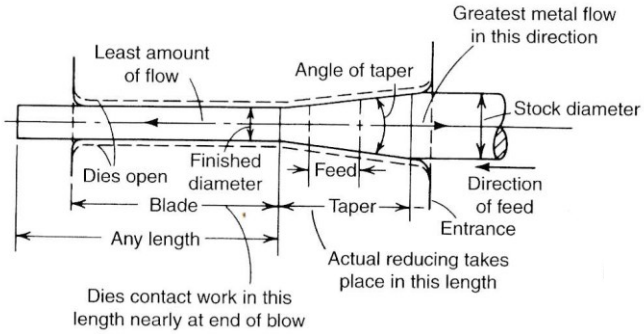

Figure 18: Effect of swaging on workpiece [30]

2.3.3 Overview of product applications

Aluminum alloy extrusion products are popularly used across a wide range of industries. As discussed in Section 1.1.3.1, aluminum alloys are so versatile because the physical and mechanical properties of aluminum alloys mean that they have a good workability that lends itself well to extrusion. The natural oxide skin on aluminum alloys gives an aesthetically pleasing finish and good corrosion resistance to the extrusion products [27]. Heat-treatable aluminum alloys, such as 2xxx, 6xxx, and 7xxx series alloys, are particularly popular because of their favourable mechanical properties.

Uses for extruded aluminum alloy products include applications in the transport industry such as components of train and subway carriages, passenger buses, car chassis, freight vehicles, and aircraft. They have also been used in watercraft as some heat-treatable aluminum alloys have excellent resistance to seawater corrosion[27]. Aluminum alloy extrusions became popular in transportation industries because of the weight savings that are made through the use of aluminum alloys instead of steels [27].

Aluminum alloys are also used in the manufacture of industrial equipment. This includes motor and machine housings that assist in cooling, the structural components of machines such as food slicing equipment and industrial-scale looms, and the pipe systems in some chemical industries. Aluminum alloy extrusions are also used in electrical equipment. Examples may be found in the manufacture of electrical pneumatic control units and heat sinks designed to remove heat from electronic equipment [27]. One such heat sink is shown in Figure 9.

Extruded aluminum alloy products are also found in architectural contexts. In 2006, the building industry accounted for 15% of the total aluminum consumption in Germany, the largest usage of aluminum and its alloys by a single industry [27]. Applications of aluminum alloy extrusions in architecture include window and door frames, central components of building architecture, and industrial staircases. Aluminum alloy extrusions may also be used for dual structural and aesthetic purposes in architectural applications, as in components of building facades. Aluminum alloy extrusions are frequently used when the front of the building is predominantly glass with supporting struts as shown in Figure 19.

Figure 19: Image showing use of aluminum extrusions in building facade[27]

2.3.4 Extrusion of sintered preforms

Extrusion processes have been used in conjunction with powder metallurgy (PM) techniques. In some PM processes, hot extrusion is a method of consolidating and densifying compacted and/or sintered powders. This is particularly useful if the material cannot be processed by conventional methods, such as casting. The technique has been successfully used in the processing of reactor materials and beryllium [27]. As a result, there is information available on the extrusion of powdered metals, but little information on the extrusion of sintered preforms. There are limited studies and literature on the extrusion of sintered PM aluminum alloy preforms.

Studies that have been carried out involving the extrusion of sintered aluminum PM alloy preforms suggest that aluminum alloys processed by PM may be successfully extruded with few observable defects[31]. Studies have also consistently reported that the extrusion processes had a strong effect on the consolidation of materials and substantially increased the density of samples[31]–[34]. In one case, researchers saw an increase from 70% of theoretical density following sintering, to 98.6% of theoretical density following a hot extrusion process [33]. Very little porosity is observed in samples which have undergone both sintering and extrusion processes.

The improved metallurgical bonding may also transpire and contribute to the improvement in mechanical properties seen in PM products that were both sintered and extruded. As with density, multiple studies have observed that mechanical properties were either comparable to or

improved from the properties of the wrought alloy equivalent[31], [32], [35]. In some cases, the improvement in mechanical properties was attributed to work hardening and dispersion strengthening effects associated with the extrusion process, but this has not been confirmed[32]. In extrusion of aluminum PM preforms, the improvement in mechanical properties may also be related further disruption of the Al_2O_3 oxide layer. The high stresses imparted by the extrusion could fracture remaining oxide layers and form a metallurgical weld between particles, further improving bonding [5].

Studies observed that a combination of sintering and extrusion processing led to the development of interesting microstructures. Generally, microstructures were observed to be elongated in the extrusion direction [36]. The microstructures were consistently fine and uniform with little or no porosity observed [32]. Hot extrusion led to a fine, layered structure which demonstrated good combination and contact between powders, consistent with the results from the density and mechanical properties [36]. Indeed, one researcher posited that extrusion could have a homogenizing effect on the material, suggesting the extrusion processing had assisted in crushing the acicular grains present in the sample that could have negatively impacted ductility [36]. Hot extrusion combined with the standard PM approach has also been shown to assist in the dissolution of alloying elements and the homogenization of the material [10]. Even when extrusion was hot, no significant coarsening of grains was observed following the process [36]. Studies have also suggested that sintered and hot extruded components may be successfully heat-treated [31]. As alluded to in Section 1.1.2.2, heat treatments are key to the development of competitive, high level mechanical properties for aluminum PM alloys[5].

Extrusion has also been used in the processing of metal matrix composite materials (MMCs) developed through a powder metallurgy approach[31], [37], [38]. Extrusion helps to ensure a homogeneous distribution of the reinforcing ceramic phase and assists in the consolidation of MMCs.

Chapter 3. Sinter-Swage Processing of an Al-Si-Mg-Cu Powder Metallurgy Alloy

M.F. Wilson[1], I.W. Donaldson[2], D.P. Bishop[1*]

1 – Dalhousie University, Department of Mechanical Engineering, 1360 Barrington Street, Halifax, NS, Canada, B3H 4R2

2 – GKN Sinter Metals, Advanced Engineering, 1670 Opdyke Court, Auburn Hills, MI, USA, 48326

*Corresponding Author: Paul.Bishop@dal.ca

Status: Submitted to Canadian Metallurgy Quarterly

The following experimental procedures, results, and discussion were completed by M.F. Wilson. Secondary authors assisted manuscript editing, and/or project supervision.

Abstract

A powder metallurgy (PM) alloy similar to wrought aluminum alloy 6013 was researched. Alloy variants emphasized systems with/without pre-alloyed manganese and admixed elemental tin powder. Systems with pre-alloyed manganese demonstrated an inferior response to die compaction and only achieved a density of 91% of theoretical after sintering. Conversely, the mixture that contained a trace addition of tin and was devoid of manganese densified to >98%. In the T6 state, this particular PM variant exhibited stiffness and yield strength that were comparable to wrought 6013-T6 but maintained a limited tensile ductility. The latter trait, as well as UTS and fatigue performance, were all improved significantly with the inclusion of a hot swaging step after sintering. As hot swaging eliminated the bulk of residual porosity in the sintered preform, this was believed to have underpinned much of the gains realized.

Keywords: Aluminum, Powder Metallurgy, Sintering, Hot Swaging, Tensile, Fatigue

3.1 Introduction

Powder metallurgy (PM) is a versatile manufacturing technology that readily accommodates high volume production of structural engineered components. PM is also conducive to processing a wide range of metallic materials including steels, copper alloys, and aluminum alloys[39]. When processing the latter, the principal stages of the process are powder production/mixing, die compaction, liquid phase sintering, and finally, post-sinter sizing to refine dimensional tolerances. This process is near-net shape, meaning that minimal post-process machining is needed before a component enters service, thereby lowering net cost as well as the amount of energy consumed in manufacturing[40].

High volume commercial applications for aluminum PM commenced in the 1990s with the fabrication of camshaft bearing caps[41]. At that point, the industry was reliant on a single alloy system denoted as AC-2014[39], [42]. Since then, the portfolio of commercially feasible aluminum PM alloy systems has expanded appreciably, with a concurrent broadening of the scope of end-use applications. The bulk of alloy development efforts have centered on systems that fall within 2xxx (Al-Cu-Mg) and 7xxx (Al-Zn-Mg) series chemistries, motivated by a desire to attain enhanced mechanical properties achievable by these alloy series. Key alloys that have emerged from this work are PM counterparts to wrought 2024[15], 2618[19], and 7075[43]. Extensive research and testing has demonstrated that these alloys respond very well to PM processing and offer significant mechanical advantages in comparison to AC-2014. Comparatively, there has been far less research effort exerted on the development of 6xxx series PM alloys (Al-Mg-Si-(Cu)). Regarded as medium strength systems, wrought 6xxx materials are generally inferior to 2xxx and 7xxx formulations in terms of hardness, tensile properties, and fatigue performance. However, they typically possess superior corrosion resistance, thermal conductivity, weldability, and formability [23]. Research into 6xxx series PM alloys has been largely limited to the development of counterparts to popular wrought alloys 6061 [44], [45] and 6063 [46].

The aluminum PM sector has also investigated thermal-mechanical working of commercial alloy systems as a means of achieving performance enhancements. Applied to sintered preforms, such processes have a capacity to remove residual porosity and fragment residual oxide networks, accruing further gains in mechanical performance. Positive outcomes have been realized in many scenarios, including the hot forging of 2xxx [47], [48], 6xxx [49], and 7xxx [50] alloys.

One of the highlights from these studies is the demonstrated capacity to produce fully dense, defect-free products from all alloy series with proper selection of process parameters. As a result, the 2xxx and 7xxx PM alloy systems investigated have demonstrated significant gains in tensile properties over their wrought counterparts, corresponding to improvements in density[47], [48], [50]. Fatigue life of the hot deformed PM 7xxx alloy product was also found to be superior to that of the equivalent wrought alloy [50]. In other works, hot extrusion of 2xxx alloys has demonstrated meaningful gains [31]. The study by Wilson et al [31] revealed the successful extrusion of a 2xxx series MMC under industrial conditions. In this work, a selection of extrusion profiles were produced with no apparent defects or residual porosity. The tensile properties of the extruded products were particularly notable, with UTS and tensile ductility of the T6-treated extruded product greatly exceeding those of the T6-treated press-and-sinter counterpart.

As this survey of literature demonstrates, 6xxx series aluminum PM alloys remain under-developed and tangible gains can be realized when sintered preforms are subjected to hot deformation/extrusion. Accordingly, this study had two linked research objectives. The first was to develop a PM counterpart to another 6xxx alloy, so as to broaden the scope of promising opportunities. Here, 6013 was the alloy system selected. In wrought form, this versatile alloy is one of the highest strength members of the 6xxx series and is frequently used in structural components, particularly for aerospace applications[51], [52]. It is also amenable to hot processing, such as forging and extrusion and is responsive to various heat treatments, including the T4, T6 and T8 tempers [23]. The second objective was to study the response of the sintered product to hot deformation and the ensuing effects on mechanical properties.

3.2 Materials

Four alloys were explored as PM counterparts to wrought 6013. Variants of the alloy were prepared with and without pre-alloyed manganese and admixed tin. Designated as PM6013-Mn, PM6013-Mn-Sn, PM6013, and PM6013-Sn, the composition of each system is shown in Table *5*.

Table 5: Comparison of targeted and measured chemistries for the PM alloys investigated.

PM Alloy	Chemistry	Al	Mn	Si	Mg	Sn	Cu
PM6013-Mn	*Target*	*Bal.*	*0.5*	*0.8*	*1.0*	*0.0*	*0.9*
	Measured	Bal.	0.52	0.83	1.1	0.05	0.93
PM6013-Mn-Sn	*Target*	*Bal.*	*0.5*	*0.8*	*1.0*	*0.5*	*0.9*
	Measured	Bal.	0.53	0.85	1.1	0.49	0.89
PM6013	*Target*	*Bal.*	*0.0*	*0.8*	*1.0*	*0.0*	*0.9*
	Measured	Bal.	0.002	0.85	1.2	0.002	1.0
PM6013-Sn	*Target*	*Bal.*	*0.0*	*0.8*	*1.0*	*0.5*	*0.9*
	Measured	Bal.	0.001	0.84	1.1	0.48	0.95

All alloys were formulated from commercially available powders. The base powder for alloys PM6013-Mn and PM6013-Mn-Sn was an aluminum powder pre-alloyed with 0.6% by weight (wt. %) manganese. Shown in Figure 20a, this powder had an average particle size of 103 μm. The base powder for alloys PM6013 and PM6013-Sn was a nominally pure aluminum powder (Figure 20b) with an average particle size of 116 μm. The raw powder mixtures were prepared using admixed additions of elemental magnesium (D_{50} = 31 μm) and tin (D_{50} = 4 μm), where applicable. Silicon and copper were sourced through the addition of master alloys. These were Al-12Si wt. % (D_{50} = 33 μm) and Al-50Cu wt. % (D_{50} = 31 μm) respectively. All powders were produced by Kymera International, with the exception of the elemental magnesium powder, which was produced through inert gas atomization (Tangshan Weihao Magnesium Powder Company Ltd.). Once the powder blends were prepared, 1.5 wt. % of LicoWax C (Clariant Corporation) was also added to all blends to allow for ease of compaction.

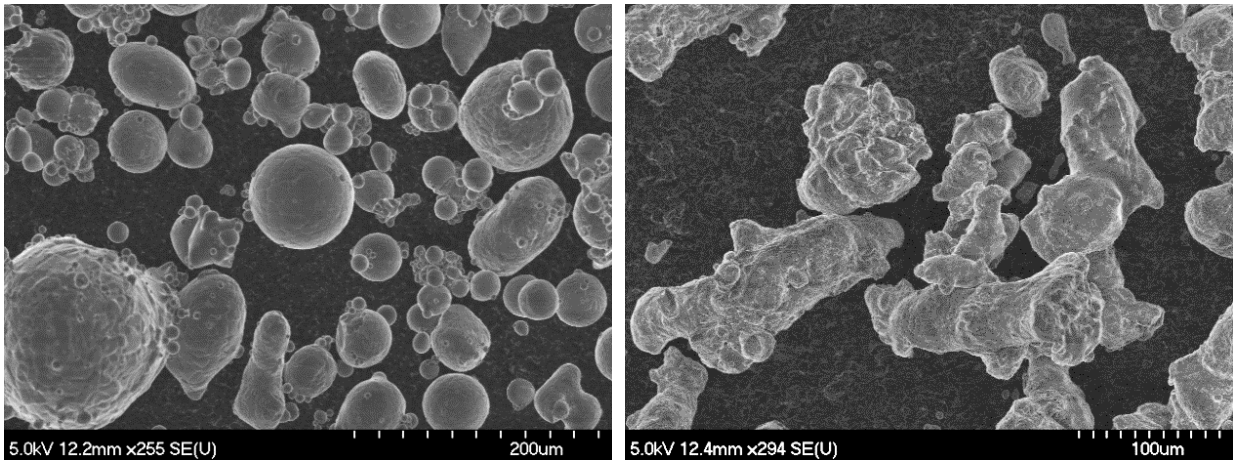

(a) (b)

Figure 20: SEM images of the base aluminum powders utilized in PM6013 variants. (a) Pre-alloyed Al-0.6Mn powder and (b) pure aluminum.

3.3 Methodology

Test specimens were prepared using a classical press and sinter PM approach coupled with post-sinter thermal-mechanical working and heat treatment. Initially, the starting powders were blended in the appropriate proportions using a Turbula shaker mixer. Alloying additions were added to the requisite base aluminum powder sequentially with a 30-minute blend time applied between each addition. Apparent density was assessed for each blend using an Arnold Meter, per MPIF Standard 48[53]. Flow rate properties were determined by passing 25 g of each powder blend through a Carney Apparatus. A rate in grams per second was calculated from this data. Samples were then die compacted at 220MPa using an Instron 5594-200HVL test frame. Three different samples geometries were fabricated. These were transverse rupture strength (TRS) samples (nominally 31.7 mm x 12.7 mm x 9.7 mm), Charpy samples (nominally 75 mm x 10 mm x 10 mm) and larger rectangular samples (nominally 20 mm x 92 mm x 10 mm). Green density was determined using a 'wet' approach, as per MPIF Standard 42 [54]. Green strength was determined using a three-point bend methodology, as outlined in MPIF Standard 15 [55]. Both were completed using TRS bars.

Green compacts were then sintered in a three-zone Lindberg tube furnace, under flowing high-purity (99.999%) nitrogen gas. The furnace atmosphere was conditioned prior to heating through multiple applications of an evacuate (10^{-2} torr) and backfill sequence prior to maintaining a static

gas flow of 9.4 litres/minute for the duration of the sinter cycle. The thermal profile consisted of a 20-minute hold at 420ºC, to allow for de-lubrication, followed by a 30-minute hold at 630ºC when sintering TRS and Charpy samples. Larger rectangular bars were held at 630ºC for 50 minutes to ensure a complete sinter. After the sintering time elapsed, samples were slid into the water-jacketed end of the tube furnace, where they were cooled to ambient temperature under the nitrogen atmosphere. TRS samples were utilized to monitor the general sintering behavior of the alloys. Data on sintered density, dimensional change, and mass change induced by sintering were compiled. To quantify dimensional change, width, length, and overall length (OAL) or thickness measurements were obtained for each sample before and after sintering. Sintered density was assessed using an oil-infiltration Archimedes approach in accordance with MPIF Standard 42[54]. Measurements of density are reported as a percentage of the theoretical full density calculated for the alloy using the approach specified by the Aluminum Association [56].

Sintered rectangular samples were machined into cylinders (18mm diameter and 90mm in length), pre-heated to 485ºC and then hot swaged in a laboratory scale apparatus. This involved a series of passes through successively smaller dies until a final diameter of 12.7 mm was achieved, representing a reduction in area of approximately 50%, for an extrusion ratio of 2:1. Samples were re-heated at 485ºC for 5 minutes between each pass. Two post-swage heat treatments were considered - T6 and T8. For the former, swaged rods were solutionized in air at 560ºC for 2 hours (Lindberg box furnace), water quenched, and then aged at 190ºC (Heratherm mechanical convection oven). To achieve the T8 condition, samples were subjected to the same solutionize/quench process but were then cold worked to achieve an average reduction in thickness of 11%, and then aged at 190ºC.

Melting behaviour of swaged specimen was assessed using a Netzsch 404 F1 differential scanning calorimeter (DSC). Temperature and sensitivity calibrations were carried out prior to testing. All tests were carried out under a conditioned atmosphere, with flowing high-purity nitrogen gas at 50 ml/min. Circular samples were machined from swaged rods (4 mm in diameter by 2 mm in thickness). Samples were heated at a rate of 20ºC/minute to 700ºC, then cooled at the same rate to ambient temperature.

Mechanical testing included the measurement of hardness, tensile properties and bending fatigue performance. Hardness data was acquired using a Wilson Rockwell 2000 tester in Rockwell

Hardness E-scale (HRE) and Rockwell Hardness B-scale (HRB). Reported values were taken as the average of four measurements. Tensile properties were assessed in accordance with ASTM Standard E8-M[57]. Here, swaged rods and Charpy bars were machined into threaded-end tensile specimen and then loaded to fracture with an Instron 5594-200 HVL load frame, equipped with a 50kN load cell and an Epsilon model 3542 extensometer. The extensometer remained attached to each sample through to failure. Reported tensile properties for T6 and T8 samples were averaged values derived from three and two test samples respectively. 3-point bending fatigue properties were assessed using the statistical staircase methodology, as per MPIF Standard 56 [58], through application of a staircase method, under a 3-point loading condition and with a 5 MPa step size. Sample geometries and standard of loading were as per MPIF Standard 41[59]. All samples were rectangular (31.7 mm x 12.7 mm x 9.7 mm) and were tested using an Instron 1332 servo-hydraulic frame equipped with an MTS 642 bend fixture that maintained a 24.7 mm span between the two bottom pins. Loading was applied at 25 Hz (R = 0.1) to a runout limit of 10^6 cycles. The 10%, 50% and 90% survival stress values were then calculated from the resultant data.

For microstructural assessments, specimens were hot mounted in conductive epoxy and then polished using a Struers Tegramin semi-automatic polisher. A standard sequence of polishing media was used, including silicon carbide papers, diamond pastes, and colloidal silica. Optical microscopy was carried out using a Zeiss Axiotech upright microscope and a Keyence VK-X1000 laser confocal microscope in optical mode. Electron microscopy was accomplished using a Hitachi S-4700 cold field emission scanning electron microscope (SEM) operated with a 20 kV accelerating voltage and 20 mA beam current. Energy-Dispersive Spectroscopy (EDS) was carried out using an Oxford Instruments X-Max 80 mm^2 EDS detector.

3.4 Results and Discussion

3.4.1 Compaction Response

To identify a reasonable PM counterpart to wrought 6013, four chemically unique alloys were considered. Each contained identical concentrations of magnesium, silicon, and copper, principally differentiated by the presence/absence of manganese and/or tin. Manganese is utilized in wrought 6013 and was instilled in two PM variants by pre-alloying it into the base aluminum powder. However, since it was understood that pre-alloying typically increases the yield strength of a powder, thereby complicating die compaction behavior, two other PM systems were devoid of manganese and utilized pure aluminum as the base powder. For each pair, one included a trace addition (0.5 wt.%) of tin, and one did not. Tin is known to catalyze the densification response of numerous aluminum PM alloys and as such, was considered for this purpose[1].

To characterize each of the blends prior to compaction, the flow and apparent density properties were assessed (Table 6). Alloys containing manganese demonstrated higher apparent densities and reduced flow rates relative to those prepared with pure aluminum as the base powder. Both of these responses may be related to the morphology of the base aluminum powder. The powder which was pre-alloyed with manganese (Figure 20a) had a spherical morphology, while the un-alloyed base powder (Figure 20b) was irregular in shape. Greater interparticle friction is generated between particles with an irregular morphology[1]. Higher interparticle friction leads to increased separation between particles, which permits fewer particles per unit volume and lowers apparent density. By this principle, the flow rate of PM6013 and PM6013-Sn should be slower than the manganese bearing alloys; it is in fact slightly faster. This may be because the slightly coarser particle size of the pure aluminum base powder allowed the particles to flow more effectively.

Table 6: Apparent density and flowrate data for 6013 PM variants.

PM Alloy	**Flow Rate** (g/s)	**Apparent Density** (g/cm^3)
PM6013-Mn	2.2 ± 0.1	1.35 ± 0.01
PM6013-Mn-Sn	2.2 ± 0.2	1.41 ± 0.01
PM6013	2.9 ± 0.1	1.15 ± 0.01
PM6013-Sn	2.8 ± 0.1	1.18 ± 0.01

The additions of tin had no statistically meaningful effect on flow rate, but were found to impart increases in apparent density. Since tin is a relatively heavy element (118.7 g/mol) even minor additions have the capacity to increase the density of a lightweight aluminum alloy to a meaningful extent. For example, as shown in Table 7, the addition of 0.5 wt. % tin increased the calculated full theoretical densities [56] by 0.09 g/cc (~3.3%). As somewhat similar gains were noted in apparent density values, it was plausible that the results were largely a direct reflection of the heavy element addition.

Data on green strength and green density were also obtained for each alloy (Table 7). Although additions of tin had no statistically meaningful effect on these attributes, significant differences were noted in the systems that employed pre-alloyed manganese. PM6013 and PM6013-Sn demonstrated an approximately four-fold increase in green strength over their manganese-bearing counterparts. As with flow and apparent density, this was principally related to differences in the morphology of the base powder particles. Particle shape is one of the most important factors affecting the green strength of a compact [7]. The spherical shape of the base powder pre-alloyed with manganese would have resulted in limited surface contact between particles, and thus an inferior green strength. In contrast, the irregular shape of the un-alloyed aluminum base powder would have manifested many opportunities for mechanical interlocking of particles upon compaction, manifested as higher green strength. Pre-alloying of the base powder with manganese would have exacerbated this effect by strengthening the spherical particles, thereby making them more resilient to the plastic deformation necessary for interlocking.

Table 7: Compaction response of 6013 PM variants.

PM Alloy	**Theoretical Density** (g/cm^3)	**Green Strength*** (MPa)	**Green Density*** (%)
PM6013-Mn	2.708	2.61 ± 0.7	93.7 ± 0.2
PM6013-Mn-Sn	2.717	2.70 ± 0.1	93.7 ± 0.2
PM6013	2.699	8.58 ± 0.4	92.1 ± 0.2
PM6013-Sn	2.708	8.76 ± 0.8	92.2 ± 0.1

* Measured from samples compacted at 220 MPa.

3.4.2 Sintering Response

Data on the general sintering response of the alloys are shown in Table 8. Although all alloys demonstrated mass losses that approximated 1.5 wt.%, corresponding to the lubricant boiling off as expected during sintering, there was considerable variation in the sintered density and the warpage that compacts experienced. Alloys containing manganese did not respond favourably to sintering. Here, sintered densities were inferior to green densities (Table 7) and compacts experienced a net swelling in all dimensions (Table 8). Alloys devoid of manganese sintered to a much greater extent. The sintered densities of these materials were >96% and had measurably improved relative to those of the starting green compacts. This improvement was consistent with dimensional changes as shrinkage in all directions was noted.

Table 8: Data on the general sintering response of 6013 PM variants.

PM Alloy	Sintered Density (%)	Mass Change (%)	Dimensional Change		
			OAL (%)	Width (%)	Length (%)
PM6013-Mn	91.1 ± 0.6	-1.41 ± 0.1	1.2 ± 0.4	0.1 ± 0.2	0.6 ± 0.2
PM6013-Mn-Sn	90.9 ± 0.1	-1.48 ± 0.1	2.0 ± 0.4	0.2 ± 0.1	0.6 ± 0.2
PM6013	96.3 ± 0.6	-1.43 ± 0.1	-4.5 ± 0.2	-1.8 ± 0.2	-0.8 ± 0.3
PM6013-Sn	98.4 ± 0.2	-1.45 ± 0.1	-4.2 ± 0.3	-2.5 ± 0.4	-1.8 ± 0.1

The addition of tin was unable to enhance the sintering response of PM6013-Mn as both swelling and a poor sintered density prevailed with its addition. However, the positive sintering response of PM6013 was further improved by the addition of tin. This may be related to the behaviour of tin during liquid phase sintering (LPS). Because tin has a lower melting point than other alloying additions, it typically forms part of the liquid phase that acts to densify the compact. Hence, the addition of tin to PM6013-Mn-Sn and PM6013-Sn could have resulted in a slightly higher liquid fraction being present during the LPS of these alloys than in PM6013-Mn and PM6013. German notes that while high liquid fraction in LPS leads to fast densification, the increased densification can cause dimensional control to become more challenging [1], [5]. However, because tin was added in trace quantity, this does not completely explain the observed effect. Aluminum powders invariably react with oxygen to form a thin layer of alumina, Al_2O_3, on the surface of the powders[5], [60]. The increased apparent density of the manganese-bearing alloys indicates tighter packing of particles, causing higher amounts of oxide to be present per unit volume than in the alloys that did not contain manganese. The inability of tin to wet alumina is a well-

documented effect[5], [61]. A difference in wetting behaviour, an important feature of LPS, may have played a role in the differences between the sintering response of the two tin-bearing alloys.

It is also interesting to note that the alloys which achieved higher green densities, PM6013-Mn and PM6013-Mn-Sn, produced a lower sinter density and therefore less densification during sintering. Theoretically, the higher green densities should be measured in the compacts that sintered better, because densification is a function of green density[5]. This was not the case here. An examination of the net change between apparent density and green density of PM6013-Mn and PM6013-Mn-Sn proves instructive in this case. PM6013-Mn and PM6013-Mn-Sn demonstrate a net change of 1.2 g/cc and 1.1 g/cc respectively between apparent density and green density. By contrast, PM6013 and PM6013-Sn show slightly higher net changes of 1.3 g/cc and 1.4 g/cc respectively. This indicates that in the compaction of PM6013-Mn and PM6013-Mn-Sn there was less material movement taking place than in the compaction of the alloys devoid of manganese. This suggests that the particles were not mechanically bonding as effectively, which is also observable in the comparatively lower green strength of these two alloys. Material movement also acts to fracture the oxide film on the powder and provide sites for metal-to-metal mechanical bonding. Because material movement is lessened there are likely fewer sites of metal-to-metal contact established between particles, which may in turn inhibit sintering. Increased interparticle contacts in PM6013 and PM6013-Sn allow these alloys to sinter more effectively.

The disparity in these two sintering responses was particularly evident microstructurally, as seen in Figure 21. Alloys PM6013-Mn and PM6013-Mn-Sn demonstrated low sinter quality. Evidence of the starting powder morphology prevailed, and many irregular and continuous pores (black features) were visible in the microstructures. These factors indicated that only early-stage sinter bonding was achieved. Conversely, samples produced without manganese sintered to a much higher quality. Raw powder particles were no longer visible and the few pores that remained were rounded and discontinuous.

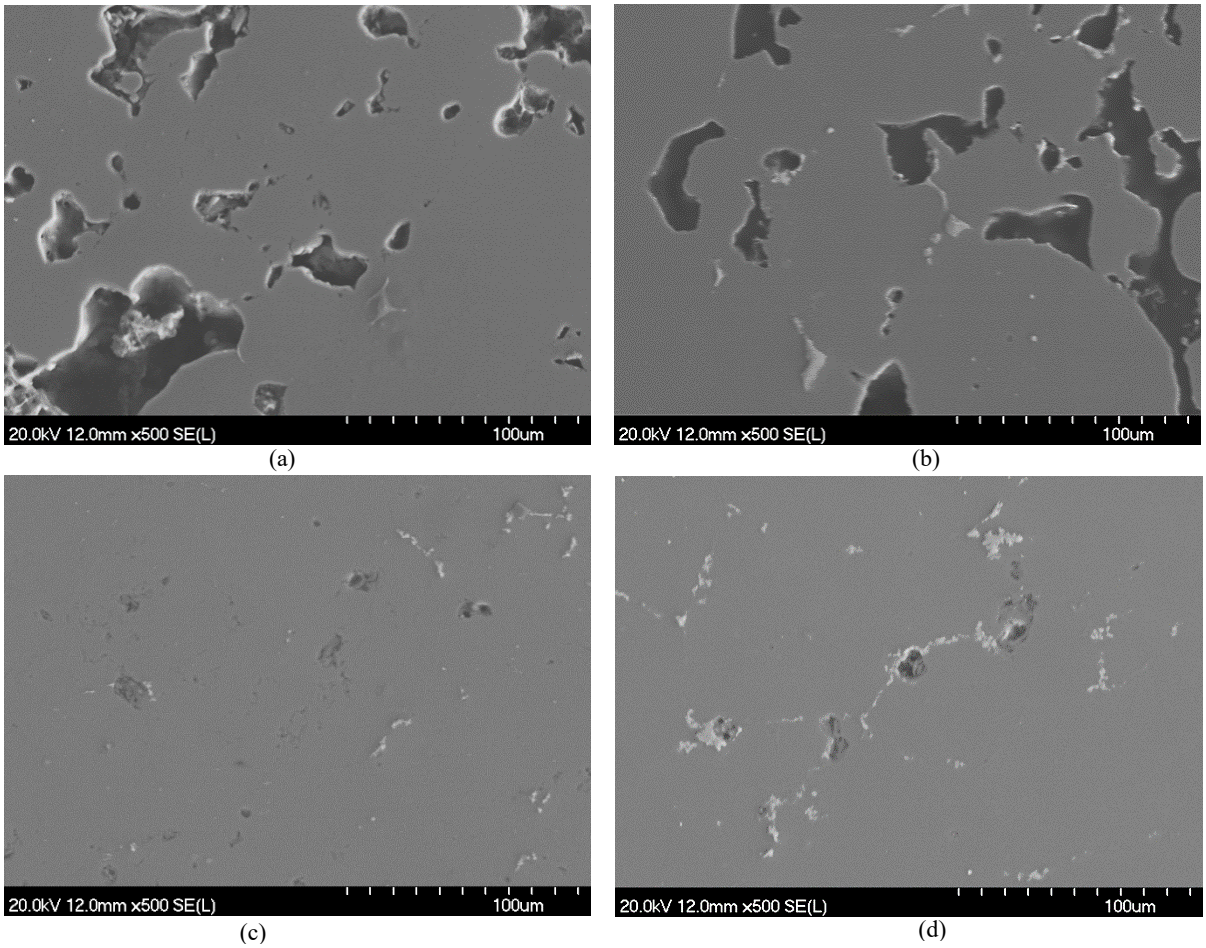

Figure 21: SEM images of the sintered microstructures observed in (a) PM6013-Mn, (b) PM6013-Mn-Sn, (c) PM6013, and (d) PM6013-Sn. All samples in the as-sintered condition.

3.4.3 Effects of Hot Swaging

Sintered bars of each alloy were then processed through hot swaging. Macroscopically, all alloys responded well, as no visible defects were evident in the finished products. Microstructurally, the effect of swaging was immediately apparent in the manganese-bearing alloys when comparing the pre- (Figure 21(a)/(b)) and post-swaged (Figure 22(a)/(b)) microstructures. Swaging closed the majority of porosity remaining in the as-sintered materials. The pores that remained were now smaller and less continuous. Because the sintered densities of PM6013 and PM6013-Sn were substantially higher, the differences between their pre- and post-swaged microstructures were less marked. However, each alloy experienced a measurable decrease in the amount of residual porosity present such that all materials were >99% of full theoretical density after swaging. Specifically, PM6013 and PM6013-Sn exhibited swaged densities of 99.5% and 99.4% of theoretical respectively. In comparison, those of PM6013-Mn and PM6013-Mn-Sn were both slightly lower at 99.1%. The marginally improved values measured for PM6013 and PM6013-Sn were attributed to their higher sintered densities (Table 8), and concomitantly, the fact that there was significantly less residual porosity to eliminate.

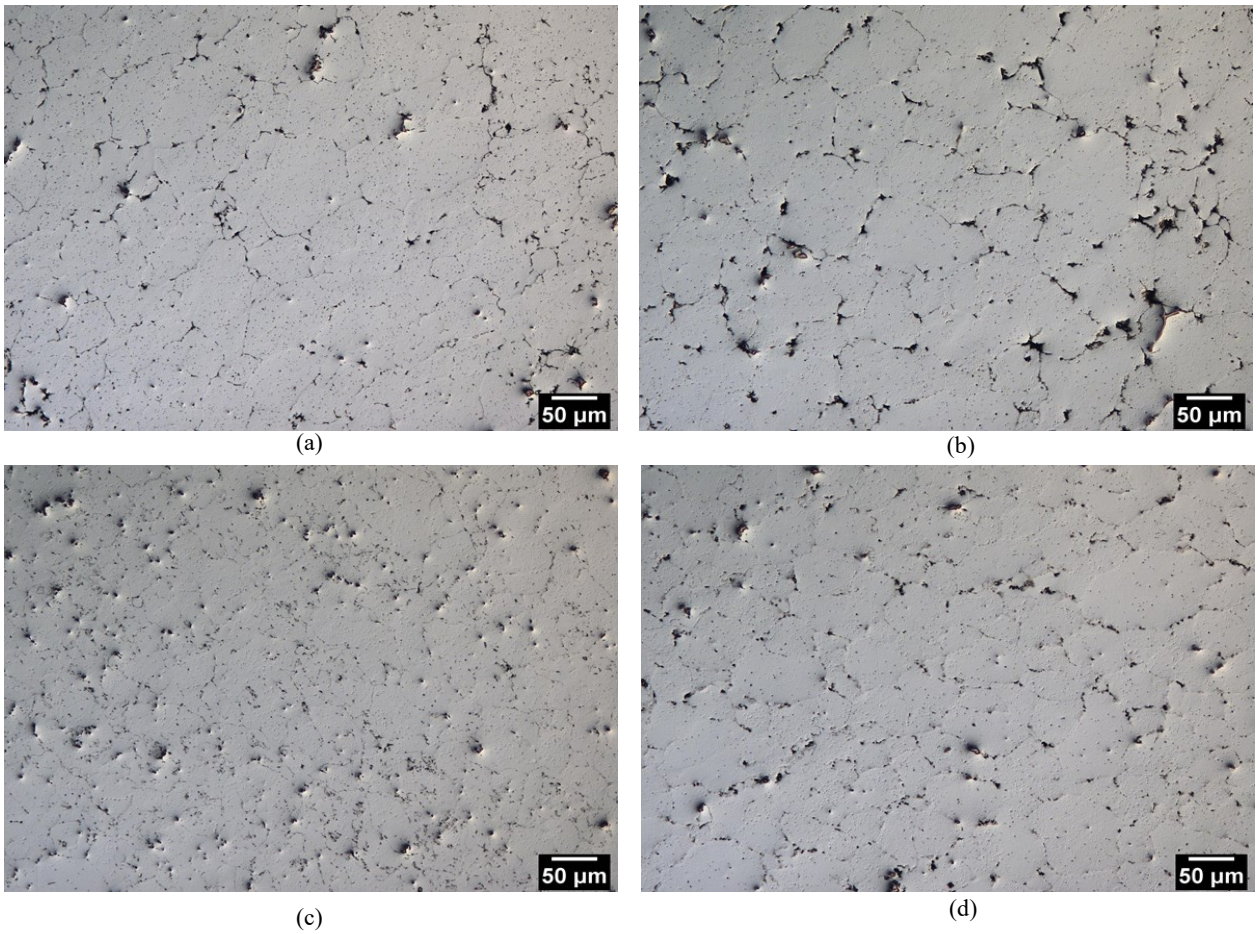

Figure 22: Microstructures of 6013 PM variants in the as-swaged condition. (a) PM6013-Mn, (b) PM6013-Mn-Sn, (c) PM6013, and (d) PM6013-Sn. All images recorded transverse to the long axis of the swaged rod.

Swaging had the effect of homogenizing the microstructures. All microstructures were dominated by white α-aluminum grains, with no evidence suggesting that the secondary intergranular phase had coarsened as a result of the heat applied during hot swaging. A minor fraction of residual porosity remained in all microstructures, consistent with swaged density measurements. Residual porosity was observed to be mainly intergranular in nature.

As in industrial extrusion operations, the grains were elongated in the direction of swaging, when viewed longitudinally[27]. Evidence of metal flow is also present when the edges of the microstructure are viewed, as would be expected from a hot deformation operation.

3.4.4 Development of Heat Treatment Parameters

Since wrought 6013 is a heat treatable alloy, the effects of T6 and T8 processes on PM6013 variants were considered. Both commence with a solutionization stage wherein the core objective is to dissolve precipitate-forming elements into solid solution. Selection of an appropriate temperature for this step is of critical importance and is frequently investigated through DSC [62]. DSC tests provide critical data on the melting behaviour of an alloy that can thereby direct research into an appropriate range of solutionizing temperatures. Heat flux traces for each PM system are shown in Figure 23. All plots show a principal melting event, labelled A. The magnitude of the peak was relatively consistent across the alloys and had an onset of ~580ºC. This event would have corresponded to bulk melting of the alloy as the temperature advanced through the semi-solid regime. Heat traces for alloys that contained tin, traces (b) and (d) in Figure 23, contained a smaller secondary event (peak B) that occurred between ~540ºC and 580ºC. It was postulated that this indicated the incipient melting of a phase containing tin. Traces (a) and (c) in Figure 23, also demonstrated a minor fluctuation around the same location as peak B. This likely indicates incipient melting in these alloys as well, however, the appreciably larger magnitude of peak B in traces (b) and (d) indicates that tin intensified the effect.

The solutionizing temperature itself needs to be above the solvus, but generally not so high that partial melting occurs. The typical solutionizing temperature of wrought 6013 is 570ºC [26]. This was below the onset of bulk melting but at the central trough of event B. Hence, the same temperature could not be arbitrarily applied to the PM systems because it could invoke liquid formation and thereby lessen the concentrations of alloying elements dissolved into solid solution. Accordingly, experimentation with a series of solutionization temperatures was needed above and below peak B. Solutionization trials at 540ºC, 560ºC, and 580ºC were selected for this purpose.

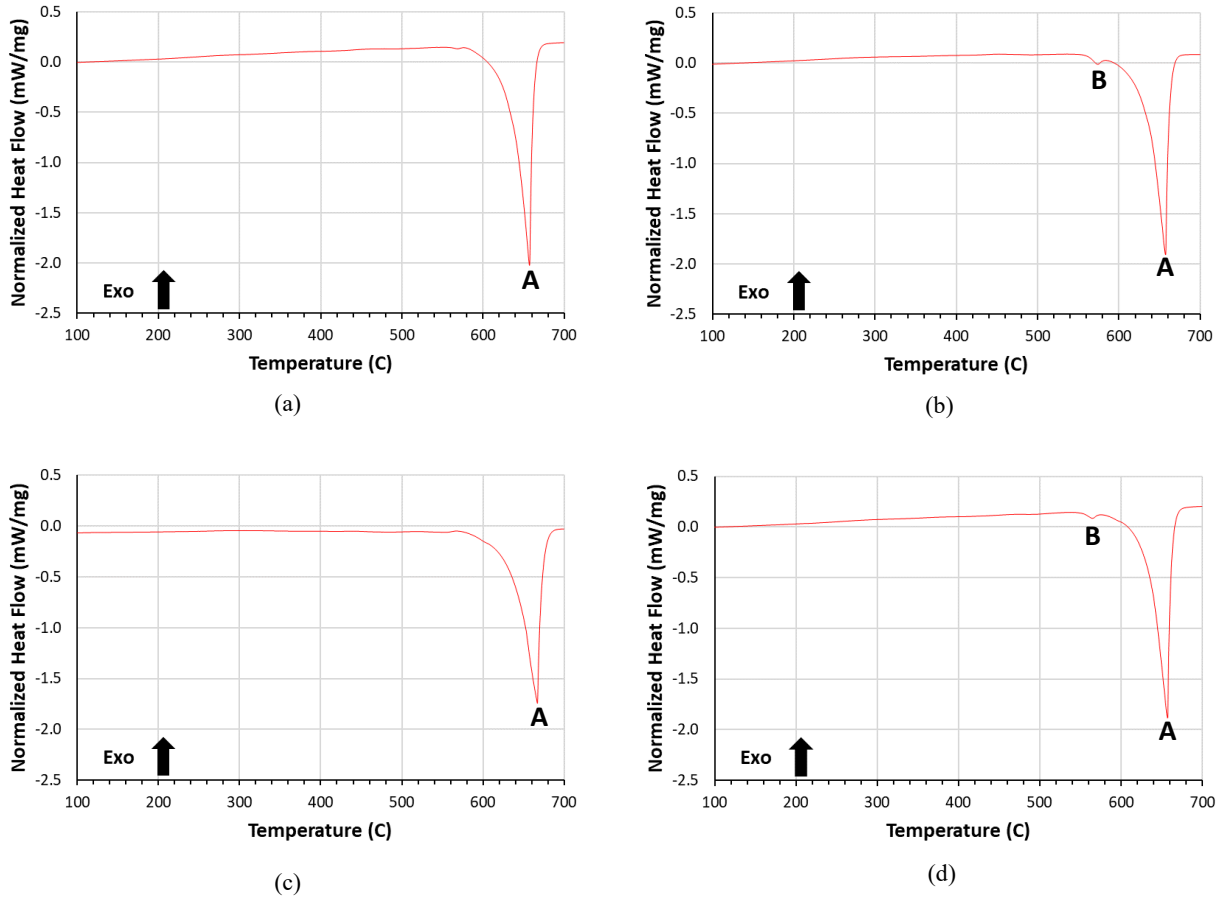

Figure 23: DSC heating traces acquired from 6013 PM variants. Labels A and B indicate melting events. (a) PM6013-Mn; (b) PM6013-Mn-Sn; (c) PM6013; (d) PM6013-Sn.

T6 aging curves were developed using the solutionizing temperatures identified through DSC assessments (Figure 24). All curves showed hardness increasing to a peak at approximately 5 hours of artificial aging. Across all alloys, 580ºC consistently produced the lowest hardness readings, suggesting a microstructure in which fewer precipitates formed. This indicates that the solutionizing temperature was excessive. There was little to separate 540ºC and 560ºC aging curves. The 560ºC aging curves demonstrated less consistency amongst the hardness readings, when compared with curves constructed at 540ºC. However, the use of 560ºC as a solutionizing temperature did produce the highest hardness readings across alloys during the construction of the aging curve. With these results, an effective T6 heat treatment cycle for all variants was solutionizing at 560ºC followed by water quenching and aging at 190ºC for 5 hours. These heat treatment parameters were used for the remainder of the investigation.

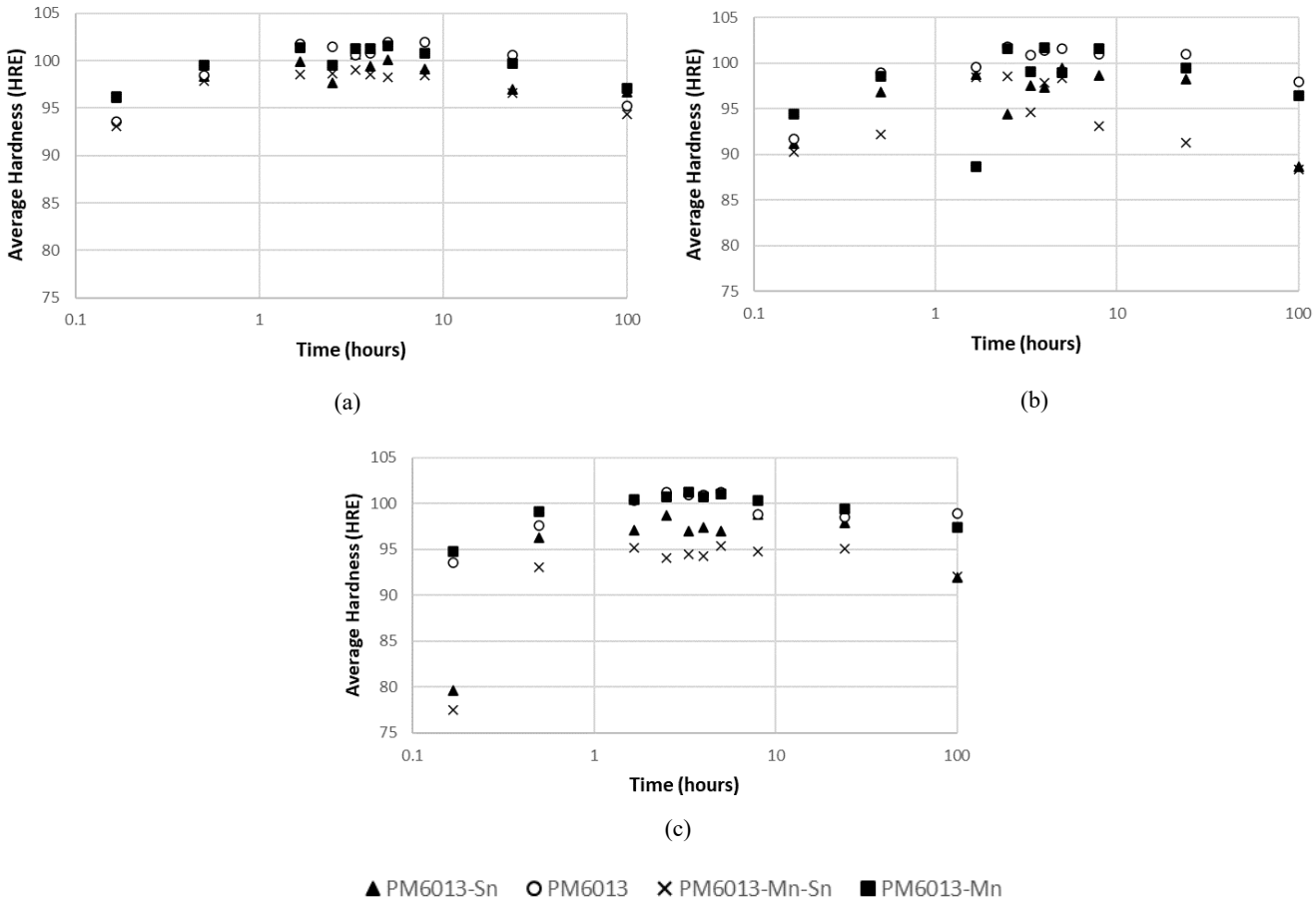

Figure 24: T6 aging curves for 6013 PM variants. Samples were sintered, hot swage, and then solutionized at (a) 540ºC, (b) 560ºC, or (c) 580ºC prior to a water quench and aging at 190ºC.

SEM images of samples in the T6 condition are shown in Figure 25. Minor fractions of residual porosity were noted in all cases, as were secondary intergranular constituents. In PM6013-Mn, the intergranular feature was light grey, relatively coarse, and, in some instances, also fractured. The latter would have been instilled during hot swaging as cracks within this feature were not observed in as-sintered micrographs (Figure 21 (a)). EDS analyses indicated that it was primarily aluminum with elevated concentrations of manganese (25 wt.%) and silicon (10 wt.%). A similar phase prevailed within PM6013-Mn-Sn, and it too showed evidence of fracture. A secondary intergranular feature was also observed in the alloy. This was brighter than the Mn-containing feature and was confirmed to be enriched in tin through EDS. As PM6013 did not contain manganese or tin, neither of the aforementioned intergranular features were observed in its microstructure (Figure 25(c)). Here, the secondary feature was finer and distributed

somewhat more uniformly throughout the microstructure. EDS indicated that it was principally aluminum with elevated, yet varying, concentrations of silicon (4-7 wt.%), magnesium (1-2 wt.%), and copper (1-4 wt.%). In PM6013-Sn, a tandem of intergranular features was once again observed. One was similar to that noted in PM6013 but now contained a minor (~1 wt.%) concentration of tin. The second was brighter and contained elevated concentrations of tin (47 wt.%) and magnesium (22 wt.%) with a balance of aluminum. No evidence of cracking was noted in any of the intergranular features within PM6013 or PM-6013-Sn.

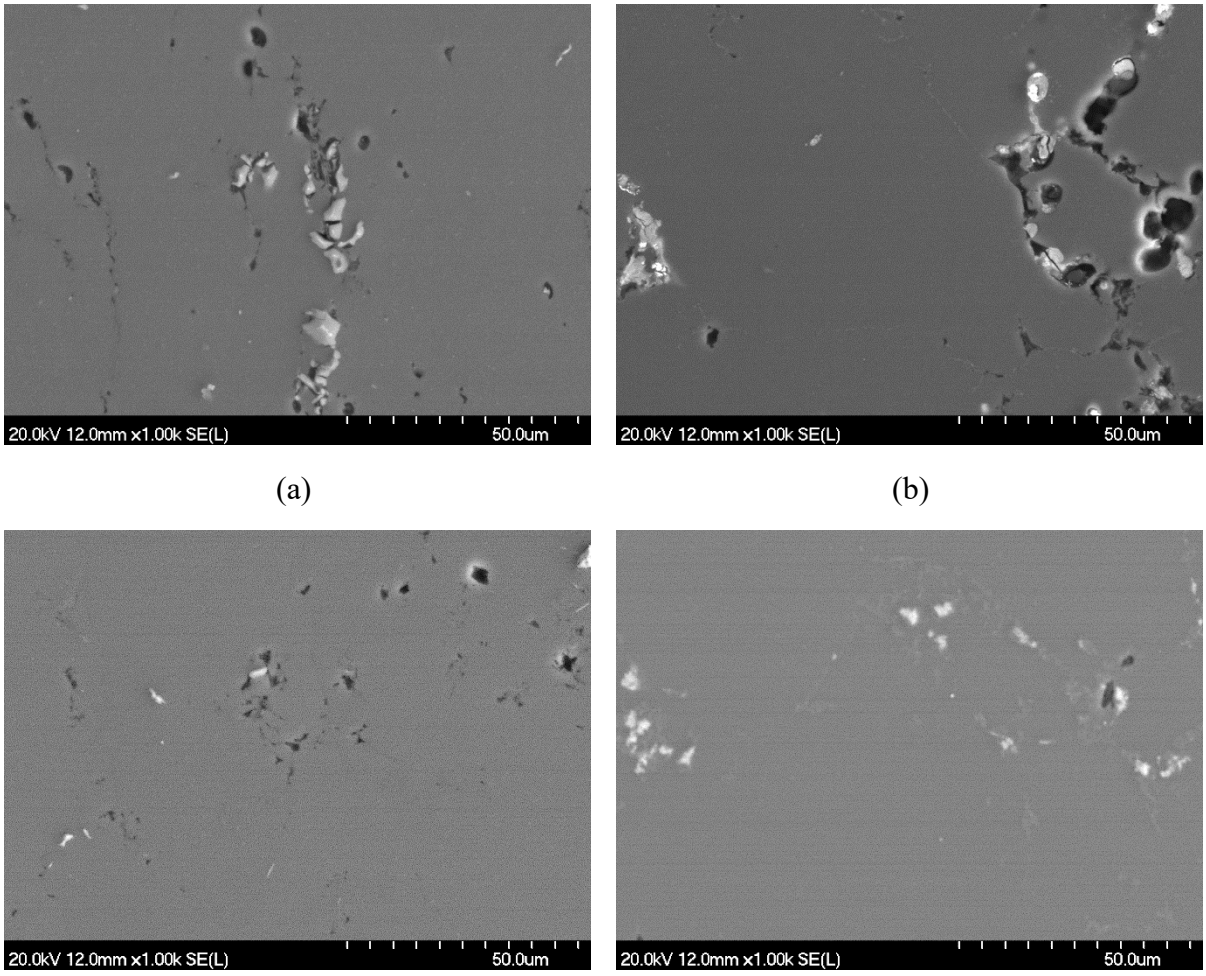

Figure 25: Microstructures of PM6013 variants processed through a sinter-swage-T6 sequence. (a) PM6013-Mn, (b) PM6013-Mn-Sn, (c) PM6013, and (d) PM6013-Sn.

An assessment of the T8 aging response was then completed. Data on hardness as a function of aging time are shown in Figure 26. All alloys were quite comparable in this regard as the peak

hardness was similar (70-76 HRB) in each instance. Generally, hardness also declined steadily with aging times beyond the first duration considered (1 hour). This behaviour indicates that the peak of the curve most likely was missed during the aging experiments. However, the difference between the true peak values and those insinuated by the data was likely minimal, as all curves exhibited a relatively shallow slope at the early stages. For the purposes of this study, 1 hour was adopted as aging time needed to achieve peak hardness in the T8 process. Samples that underwent T6 treatment demonstrated peak hardness values of 65-76 HRB (i.e., 98-101 HRE). Hence, the peak values recorded in T8 samples were rather similar to those achieved through T6 processing.

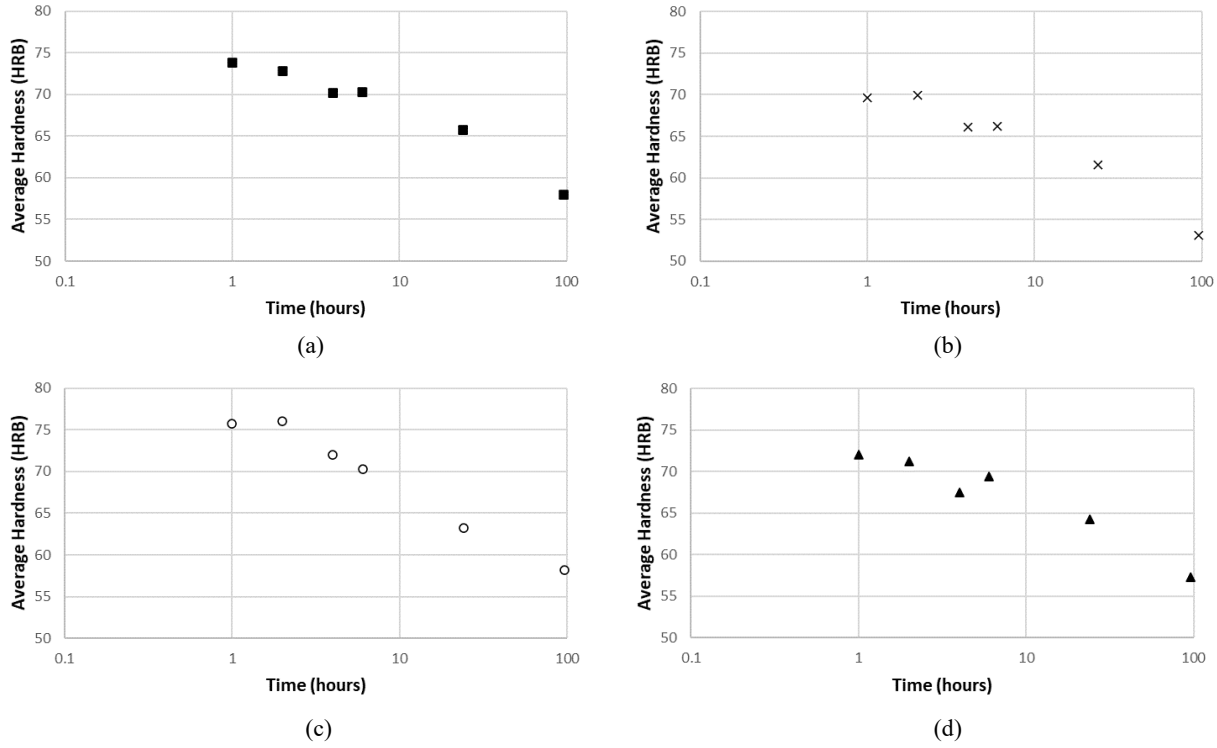

Figure 26: T8 aging curves for (a) PM6013-Mn, (b) PM6013-Mn-Sn, (c) PM6013, and (d) PM6013-Sn. Samples were sintered, hot swaged, solutionized at 560ºC, water quenched, cold worked, and then aged at 190ºC for the times indicated.

SEM images were obtained for all samples in the T8 condition (Figure 27). In each case the T8 microstructure was remarkably similar to its T6 counterpart (Figure 25). The only difference noted was with PM6013-Mn. Here, cracking was no longer limited to the boundaries of the

intergranular feature but now extended throughout the microstructure as sporadic fractures several hundred microns in length. This was ascribed to the cold working stage of the T8 process.

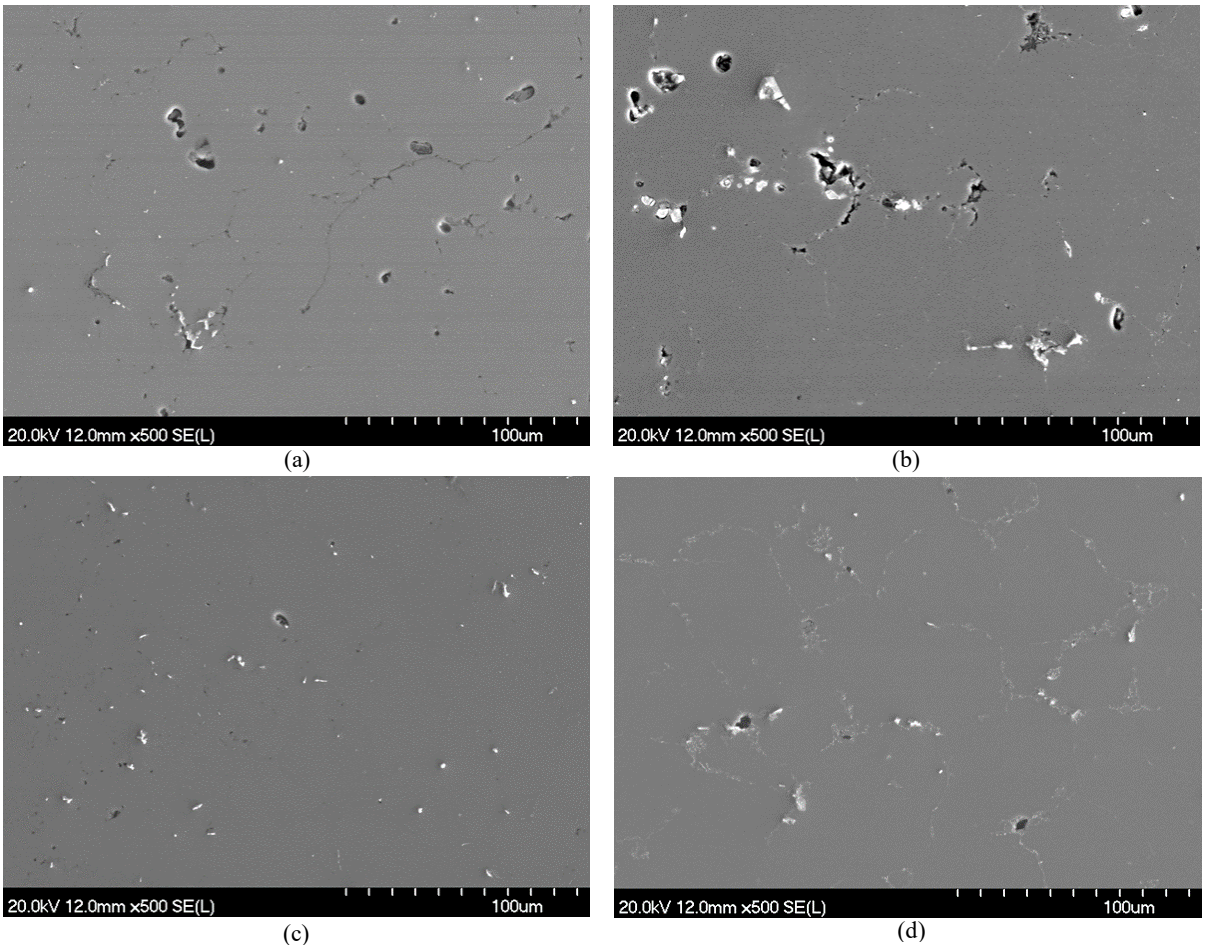

Figure 27: Microstructures of PM6013 variants processed through a sinter-swage-T8 sequence. (a) PM6013-Mn, (b) PM6013-Mn-Sn, (c) PM6013, and (d) PM6013-Sn.

3.4.5 Tensile Behaviour

With heat treatment parameters established, the focus of the study shifted to an assessment of the tensile properties of each alloy system in the T6 and T8 tempers, including the effect of swaging. Those measured for the materials in a press-sinter-T6 state are shown in Table 9. Properties of wrought alloy 6013 in a T6 temper are included to facilitate comparison. All PM systems under-performed relative to the wrought counterpart, but the differences were most acute for those that contained pre-alloyed manganese. These materials exhibited exceptionally low values for all properties as a direct result of the heightened levels of residual porosity present in them (Table 8). PM6013 and PM6013-Sn, in contrast, performed better in terms of stiffness and yield strength, as these particular properties were within ~10% of the typical wrought values. The UTS of PM6013 was appreciably lower than wrought, but was improved in PM6013-Sn. Press-and-sinter samples produced an average tensile ductility approximately 13 times lower than typical wrought values. This stark difference may be attributed to the presence of residual porosity in all the PM systems [63], which is largely absent from the wrought alloy. Overall, PM6013-Sn exhibited the most desirable T6 tensile properties confirming the beneficial role of tin.

Table 9: Tensile behaviour of PM 6013 variants processed through a sinter-T6 sequence. Typical properties for wrought 6013-T6 [25] included for comparison purposes.

Alloy	**Processing**	**E** (GPa)	**Yield Strength** (MPa)	**UTS** (MPa)	**Ductility** (%)
6013	Wrought	70	368	399	11
PM6013-Mn	Press-and-Sinter	42 ± 5	244 ± 3	245 ± 3	0.8 ± 0.1
PM6013-Mn-Sn	Press-and-Sinter	48 ± 1	149 ± 6	150 ± 6	0.4 ± 0.1
PM6013	Press-and-Sinter	62 ± 1	328 ± 4	328 ± 4	0.7 ± 0.1
PM6013-Sn	Press-and-Sinter	74 ± 3	342 ± 2	376 ± 3	1.4 ± 0.1

With the addition of a swaging step to the processing sequence, the performance gap between wrought 6013 (Table 9) and all PM variants (Table 10) narrowed dramatically. Improvements to the 0.2% offset yield strength and UTS of all PM systems were particularly acute, such that these properties were essentially equivalent to the wrought counterpart. Gains in ductility were noted as well, yet none of the PM systems achieved net values that matched the wrought threshold. On

average, the swaged-T6 PM samples demonstrated an approximately 9-fold increase in ductility over those which had been processed by sinter-T6 (Table 9).

Table 10: Tensile behaviour of PM6013 variants processed through a sinter-swage-T6 sequence.

Alloy	**E** (GPa)	**Yield Strength** (MPa)	**UTS** (MPa)	**Ductility** (%)
PM6013-Mn	66 ± 1	373 ± 2	417 ± 2	7.9 ± 0.1
PM6013-Mn-Sn	79 ± 11	345 ± 1	391 ± 1	6.6 ± 0.3
PM6013	67 ± 4	358 ± 3	410 ± 1	6.6 ± 0.7
PM6013-Sn	72 ± 1	351 ± 1	400 ± 1	9.6 ± 0.5

Hot swaging reduced the levels of residual porosity in all PM materials, but was unable to eliminate it entirely. This effect would have underpinned the remarkable gains achieved, but also the inability of PM systems to maintain a ductility that matched wrought 6013 as the remaining pores would have served as sites for crack initiation thereby limiting net ductility. Hot swaging would have contributed to the improvement in ductility through the disruption of the semi-continuous oxide network that is typically present in sintered products as well. During sintering, the alumina shell present on the surface of raw aluminum powders, reacts with magnesium to form spinel crystallites ($MgAl_2O_3$)[12]. This brittle ceramic remains throughout the sintered product and decreases tensile ductility. Hot forging has been observed to disrupt the spinel network, and thereby improve tensile ductility. It is reasonable to posit that the same mechanism engaged here. It is also notable that the fractured intergranular phases observed in Figure 25a and b did not appear to degrade ductility significantly. Other tensile properties remained relatively consistent across all four alloys. Collectively, PM6013-Sn was identified as the PM alloy that offered the best overall combination of properties; highest ductility coupled with yield strength, UTS, and stiffness values that were competitive with wrought.

Data on PM6013 systems processed through a sinter-swage-T8 sequence are shown in Table 11. These particular materials demonstrated the highest yield strength and UTS of all sequences considered and there were no significant trends observed with the presence/absence of manganese or tin. The heightened values came at the expense of modest losses in tensile ductility relative to materials subjected to a sinter-swaged-T6 process. The decrease can be attributed, in part, to the cold working stage of the T8 heat treatment, as this would have increased the concentration of dislocations present so as to invoke strain hardening and a concomitant decline

in ductility. The nature and distribution of the precipitates should have changed as a result of the T8 treatment and also been a factor of influence. In this sense, cold working can change the rate and degree of hardening that occurs because precipitates can preferentially nucleate on dislocations, thus increasing their concentration within the microstructure [26]. The additional strengthening imparted by this change could have been accompanied by a decrease in ductility. Overall, the lowest ductility was noted in PM6013-Mn. This was presumably underpinned by the aforementioned mechanisms coupled with cracks noted in the microstructure (Figure 27a).

Table 11: Tensile behaviour of PM6013 variants processed through a sinter-swage-T8 sequence.

Alloy	**E** (GPa)	**Yield Strength** (MPa)	**UTS** (MPa)	**Ductility** (%)
PM6013-Mn	69 $\pm$ 1	415 $\pm$ 1	422 $\pm$ 1	3.4 $\pm$ 0.6
PM6013-Mn-Sn	69 $\pm$ 2	408 $\pm$ 2	409 $\pm$ 2	5.6 $\pm$ 0.1
PM6013	71 $\pm$ 1	399 $\pm$ 2	431 $\pm$ 2	7.3 $\pm$ 0.1
PM6013-Sn	72 $\pm$ 1	404 $\pm$ 4	409 $\pm$ 3	7.7 $\pm$ 0.3

In summary, PM systems processed through sinter-swage-T6/T8 sequences performed relatively well in comparison with wrought 6013. In particular, PM6013-Sn most closely approximated properties attained by wrought and outperformed all of the other PM alloys with respect to tensile ductility regardless of the processing sequence employed. As such, the final stage of fatigue assessment was focused exclusively on this specific PM system.

3.4.6 Fatigue Behaviour

Data on the fatigue performance of PM6013-Sn are shown in Table 12 for the three processing sequences considered. The sinter-T6 product exhibited the lowest resistance to fatigue loading. Inclusion of a hot swaging step (i.e., sinter-swage-T6) led to a 102MPa (~68%) increase in the median bending fatigue strength. This was significant but not surprising as hot swaging addresses two factors know to have a negative impact on fatigue - residual porosity and the oxide network present. Considering the former, fatigue generally increases exponentially with density and even a small reduction in the volume fraction of residual porosity can have a significant impact[50] by lowering the number of sites available for crack nucleation and growth[7], [20], [63]. Hence, although the improvement in density of PM6013-Sn as a result of swaging was comparatively small (~1%) the net impact on fatigue would have been decisively positive. For the latter, the disruption of the oxide network through hot swaging, as discussed in Section 3.4.5, contributed to the improvement in fatigue resistance in the same manner as it improved tensile ductility. The dispersion of fine particles of the brittle spinel phase throughout the material lowers sites for crack nucleation and provides additional strengthening through the engagement of a mechanism analogous to the strengthening present in an MMC.

Table 12: Data on the 3-point bending fatigue response of PM6013-Sn systems.

Processing Sequence	$\sigma_{a,10}$ (MPa)	$\sigma_{a,50}$ (MPa)	$\sigma_{a,90}$ (MPa)
Sinter-T6	160	150	140
Sinter-Swage-T6	260	252	243
Sinter-Swage-T8	248	215	181

Specimens from the sinter-swage-T8 process also maintained an appreciable improvement over the sinter-T6 material (~43% increase) for the same reasons noted above. However, they were also inferior (~15%) to sinter-swage-T6 products. The reduced ductility of the T8 sample observed in the tensile properties likely contributed to these results.

3.5 Conclusions

Through the work completed in this study, the following conclusions were reached:

- Pre-alloying the base aluminum powder with manganese degraded compaction and sintering behaviour.
- All PM alloys responded well to hot swaging as they achieved near theoretical densities (>99% of full theoretical) with a visual absence of defects.
- The addition of hot swaging to the processing sequence manifested meaningful increases in yield strength, UTS, ductility, and fatigue performance for materials in the T6 and T8 tempers.
- Sinter-swage-T6 PM6013-Sn was the best system overall in terms of its response to PM processing and comparability in mechanical properties to wrought 6013-T6.

Chapter 4. Research Summary and Conclusions

In summary, four alloys were considered as PM equivalents to wrought alloy 6013. These were denoted PM6013-Mn, PM6013-Mn-Sn, PM6013, and PM6013-Sn. Major alloying additions of silicon, magnesium and copper were held constant across these materials, while trace additions of manganese and tin were varied. Manganese was instilled through the use of pre-alloyed aluminum powder, while tin was added elementally.

First, the compaction response of these alloys was assessed. This consisted of preliminary measurements of apparent density and flowrate of the raw powder blends. Once compaction was completed, green density and strength measurements were taken. The morphology of powders was considered to be the primary driver in the differences observed in these measurements across the alloys.

Following compaction, the sintering response of the alloys was assessed. Manganese-bearing alloys, PM6013-Mn and PM6013-Mn-Sn were found to respond poorly to sintering. Microstructural examinations revealed many continuous pores with powder particles evident. In contrast, PM6013 and PM6013-Sn sintered more successfully, producing microstructures indicative of high sinter quality. As with the compaction response, powder morphology was thought to have a significant effect on the sintering response of the alloys. Differences in wetting behaviour were also considered to be relevant to the disparity in sintering response.

Despite differences in compaction and sintering outcomes, all alloys responded well to hot swaging. No defects were observed in swaged samples and all alloys experienced an increase in density. Residual porosity was predominantly intergranular.

DSC heat traces developed for all alloys indicated the occurrence of a minor incipient melting event prior to the major bulk melting event, consistent with most 6xxx series alloys. The presence of the minor incipient melting event prompted the examination of the most appropriate T6 heat treatment parameters for the alloys. Investigations found that the best parameters were a solutionizing phase at 560°C, followed by a 5-hour aging sequence at 190°C to achieve peak hardness. Microstructural observations in the T6 condition included minor remaining porosity and intergranular phases. The presence and composition of the intergranular phases varied with

the manganese and tin content of the alloy. Cracking of the intergranular features was observed in PM6013-Mn and PM6013-Mn-Sn. An investigation was also carried out to establish T8 heat treatment parameters. Peak hardness was observed after 1 hour of aging at 190°C, following solutionizing at 560°C. Few differences were noted between T6 and T8 microstructures, except for the presence of cracking in the case of PM6013-Mn.

To assess the mechanical properties of the alloys and the effect of swaging, tensile testing was carried out. Samples were investigated in three conditions. These were press-and-sinter-T6, sinter-swage-T6, and sinter-swage-T8. Samples in the T6 condition were also compared to wrought 6013-T6. Press-and-sinter samples were found to perform poorly overall, particularly in tensile ductility, producing measurements 13 times lower than wrought values. PM6013-Mn and PM6013-Mn-Sn were also noticeably poorer in strength categories than PM6013 and PM6013-Sn. Hot swaging improved the tensile properties of all alloys. This effect was attributed to the decreased presence of pores and the disruption of the residual oxide network. Tensile ductility of the sinter-swage samples remained inferior to wrought values, but demonstrated a 9-fold increase over press-and-sinter samples. Samples in the sinter-swage-T8 condition demonstrated a slight increase in strength over their T6 counterparts, at the expense of a loss of ductility. This was largely attributed to the effects of strain hardening. Overall, PM6013-Sn offered the best combination of properties in comparison to wrought 6013.

Because of its strong tensile performance, PM6013-Sn was additionally investigated for fatigue behaviour. The same three processing conditions utilised in tensile testing were considered for fatigue. As with tensile ductility, samples in the press-and-sinter-T6 condition exhibited the lowest response to fatigue. The addition of swaging to the processing sequence resulted in a 68% increase in fatigue survival stress. Again, this is likely the result of the closing of the porosity combined with the disruption of the residual oxide network. Specimens in the sinter-swage-T8 condition exhibited an improvement over the sintered material, because of the addition of swaging, but fatigue survival stress decreased compared with sinter-swage-T6 results. This was consistent with the reduced ductility of T8 samples observed during tensile testing.

To conclude, through a comparison of four PM alloys, PM6013-Sn was selected as an equivalent to wrought alloy 6013. PM6013-Sn demonstrated the strongest sintering response of the four

alloys explored. This translated to superior mechanical properties compared with the performance of the other alloy options. PM6013-Sn responded well to hot deformation in the form of swaging. In the swaged condition, the strength properties of PM6013-Sn corresponded closely to those of wrought alloy 6013. The tensile ductility of PM6013-Sn continued to be inferior to that of wrought 6013 but did demonstrate substantial gains over sintered samples. Results of fatigue testing also indicated the benefits of hot deformation on mechanical properties. PM6013-Sn is perceived to be a viable candidate for further exploration of industrial hot deformation operations, such as hot forging.

4.1 Future Work

Further research recommendations include:

1. Further investigation of the T8 aging curve of PM6013-Sn to more accurately identify peak-aged condition. Once this was complete, the mechanical properties of PM6013-Sn in T8 condition could be re-evaluated.
2. An investigation of the fatigue performance of wrought 6013, to provide a comparator with the swaged material.
3. Characterization of the thermal properties of PM6013-Sn in the press-and-sinter and sinter-swage conditions to facilitate comparison with wrought 6013.
4. Industrial hot forging trials using PM6013-Sn. Such an investigation could include an exploration of flow stress curves and optimum parameters for the processing of PM6013-Sn. Parameters could include hot forging speed, hot forging pressure, and billet temperature.

References

[1] R. M. German, *Powder Metallurgy Science*, 2nd ed. Princeton, New Jersey: Metal Powder Industries Federation, 1994.

[2] P. Ramakrishnan, Ed., *Powder Metallurgy for Automotive and Engineering Industries*. Mumbai: Narosa Publishing, 2009.

[3] D. P. Bishop, W. F. Caley, G. J. Kipouros, R. L. Hexemer, and I. W. Donaldson, "Powder metallurgy processing of 2xxx and 7xxx series Aluminium alloys," *Can. Metall. Q.*, vol. 50, no. 3, pp. 246–252, 2011, doi: 10.1179/1879139511Y.0000000003.

[4] M. Qian and G. B. Schaffer, "Sintering of aluminium and its alloys," in *Sintering of advanced materials: Fundamentals and processes*, Z. Zak Fang, Ed. Cambridge: Woodhead Publishing Limited, 2010, pp. 291–323.

[5] S. H. Huo, M. Qian, G. B. Schaffer, and E. Crossin, "Aluminium powder metallurgy," in *Fundamentals of Aluminium Metallurgy: Production, Processing and Applications*, R. N. Lumley, Ed. Woodhead Publishing Limited, 2010, pp. 655–701.

[6] J. F. Flumerfelt, "Aluminum powder metallurgy processing," Iowa State University, 1998.

[7] Various, *ASM Handbook 7: Powder Metallurgy*, 2nd ed. Cleveland, Ohio: ASM International, 2015.

[8] K. H. . Buschow, *Encyclopedia of Materials Science and Technology*. Amsterdam: Elsevier Ltd, 2001.

[9] L. N. Smith, *A Knowledge-based System for Powder Metallurgy Technology*. London: Professional Engineering Publishing Ltd, 2003.

[10] R. M. German, *Sintering Theory and Practice*. New York: John Wiley & Sons, 1996.

[11] R. M. German, *Particle Packing Characteristics*. Princeton, New Jersey: Metal Powder Industries Federation, 1989.

[12] G. B. Schaffer, T. B. Sercombe, and R. N. Lumley, "Liquid phase sintering of aluminium alloys," *Mater. Chem. Phys.*, vol. 67, no. 1, pp. 85–91, 2001.

[13] R. M. German, P. Suri, and S. J. Park, “Review: Liquid phase sintering,” *J. Mater. Sci.*, vol. 44, no. 1, pp. 1–39, 2009, doi: 10.1007/s10853-008-3008-0.

[14] S.-J. L. Kang, “Liquid phase sintering,” in *Sintering of advanced materials: Fundamentals and processes*, 1st ed., Z. Z. Fang, Ed. Oxford: Woodhead Publishing Limited, 2010.

[15] C. D. Boland, R. L. Hexemer, I. W. Donaldson, and D. P. Bishop, “Industrial processing of a novel Al-Cu-Mg powder metallurgy alloy,” *Mater. Sci. Eng. A*, vol. 559, pp. 902–908, 2013, doi: 10.1016/j.msea.2012.09.049.

[16] A. D. P. LaDelpha, H. Neubing, and D. P. Bishop, “Metallurgical assessment of an emerging Al-Zn-Mg-Cu P/M alloy,” *Mater. Sci. Eng. A*, vol. 520, no. 1–2, pp. 105–113, 2009, doi: 10.1016/j.msea.2009.05.039.

[17] L. J. B. Smith, S. F. Corbin, R. L. Hexemer, I. W. Donaldson, and D. P. Bishop, “Development and processing of novel aluminum powder metallurgy materials for heat sink applications,” *Metall. Mater. Trans. A Phys. Metall. Mater. Sci.*, vol. 45, no. 2, pp. 980–989, 2014, doi: 10.1007/s11661-013-2011-5.

[18] D. W. Heard, I. W. Donaldson, and D. P. Bishop, “Metallurgical assessment of a hypereutectic aluminum-silicon P/M alloy,” *J. Mater. Process. Technol.*, vol. 209, no. 18–19, pp. 5902–5911, 2009, doi: 10.1016/j.jmatprotec.2009.07.007.

[19] R. W. Cooke, R. L. Hexemer, I. W. Donaldson, and D. P. Bishop, “Press-and-sinter processing of a PM counterpart to wrought aluminum 2618,” *J. Mater. Process. Technol.*, vol. 230, pp. 72–79, 2016, doi: 10.1016/j.jmatprotec.2015.11.011.

[20] E. L. Rooy, J. R. Pickens, R. S. James, A. L. Kearney, J. W. Bray, and R. B. C. Cayless, “Aluminum and Aluminum Alloys,” in *ASM Metals Handbook, Vol 02 Properties and Selection: Nonferrous Alloys and Special-Purpose Materials*, Materials Park, Ohio: ASM International, 1990, pp. 17–759.

[21] J. Snodgrass and J. Moran, “Corrosion Resistance of Aluminum Alloys,” in *Corrosion: Fundamentals, Testing, and Protection*, Materials Park, Ohio: ASM International, 2018.

[22] J. H. Hatch, Ed., *Aluminum: Properties and Physical Metallurgy*. Materials Park, Ohio: American Society for Metals, 1984.

[23] W. F. Smith, *STRUCTURE AND PROPERTIES OF ENGINEERING ALLOYS McGraw-Hill Series in Materials Science and Engineering*, 2nd ed. New York: McGraw-Hill Inc, 1993.

[24] S. W. Nam and D. H. Lee, "The effect of Mn on the mechanical behavior of Al alloys," *Met. Mater. Int.*, vol. 6, no. 1, pp. 13–16, 2000, doi: 10.1007/BF03026339.

[25] ASM International, *Atlas of Stress-Strain Curves*, 2nd ed. Materials Park, Ohio: ASM International, 2002.

[26] C. R. Brooks, "Heat Treating of Nonferrous Alloys," in *ASM Handbook Vol 4: Heat Treating*, Materials Park, Ohio: ASM International, 1991, pp. 1826–2123.

[27] M. Bauser, G. Sauer, and K. Siegert, Eds., *Extrusion*, 2nd ed. Materials Park, Ohio: ASM International, 2006.

[28] S. L. Semiatin, Ed., "Other Bulk Forming Processes," in *ASM Handbook Vol 14: Forming and Forging*, 9th ed., ASM International, 1993, pp. 680–781.

[29] M. Groover, *Fundamentals of Modern Manufacturing Materials,Processes and Systems*. 2010.

[30] B. Fluth, A. L. Hoffmanner, R. Kell, D. Hack, and W. Perun, "Rotary Swaging of Bars and Tubes," in *ASM Handbook Vol 14A: Bulk Forming*, S. L. Semiatin, Ed. Materials Park, Ohio: ASM International, 2005, pp. 156–171.

[31] M. F. Wilson *et al.*, "Hot Extrusion of a Commercial Aluminum Powder Metallurgy Metal Matrix Composite Material," *Mater. Perform. Charact.*, vol. 9, no. 4, pp. 498–513, 2020, doi: 10.1520/MPC20190161.

[32] K. Bharath, A. Mandal, A. Karmakar, A. K. Khanra, and M. J. Davidson, "Understanding the effect of hot extrusion on the evolution of microstructure and associated mechanical properties in sintered Al-Cu-Mg alloys," *Mater. Charact.*, vol. 170, no. 1, p. 110715, 2020, doi: 10.1016/j.matchar.2020.110715.

[33] M. M. El-Sayed Seleman, M. M. Z. Ahmed, and S. Ataya, "Microstructure and mechanical properties of hot extruded 6016 aluminum alloy/graphite composites," *J.*

Mater. Sci. Technol., vol. 34, no. 9, pp. 1580–1591, 2018, doi: 10.1016/j.jmst.2018.03.004.

[34] W. W. Yang, Z. M. Guo, H. Q. Cao, J. Luo, and A. P. Ye, "Fabrication and mechanical properties of high-performance aluminum alloy," *Rare Met.*, vol. 33, no. 4, pp. 400–403, 2014, doi: 10.1007/s12598-014-0262-y.

[35] P. Ashwath *et al.*, "Processing and characterization of extruded 2024 series of aluminum alloy," *Mater. Today Proc.*, vol. 5, no. 5, pp. 12479–12483, 2018, doi: 10.1016/j.matpr.2018.02.228.

[36] E. R. Wang, X. D. Hui, S. S. Wang, Y. F. Zhao, and G. L. Chen, "Microstructure and mechanical properties of Al-Si-Ni-Ce alloys prepared by gas-atomization spark plasma sintering and hot-extrusion," *Mater. Sci. Eng. A*, vol. 528, no. 18, pp. 5764–5771, 2011, doi: 10.1016/j.msea.2011.03.102.

[37] R. Deaquino-Lara, I. Estrada-Guel, G. Hinojosa-Ruiz, R. Flores-Campos, J. M. Herrera-Ramírez, and R. Martínez-Sánchez, "Synthesis of aluminum alloy 7075-graphite composites by milling processes and hot extrusion," *J. Alloys Compd.*, vol. 509, no. 1, pp. S284–S289, 2011, doi: 10.1016/j.jallcom.2010.11.183.

[38] R. Flores-Campos, I. Estrada-Guel, M. Miki-Yoshida, R. Martínez-Sánchez, and J. M. Herrera-Ramírez, "Microstructure and mechanical properties of 7075 aluminum alloy nanostructured composites processed by mechanical milling and indirect hot extrusion," *Mater. Charact.*, vol. 63, pp. 39–46, 2012, doi: 10.1016/j.matchar.2011.10.014.

[39] MPIF, "Materials Standards for PM Structural Parts," MPIF 35, 2016.

[40] J. Mascarenhas, "Powder Metallurgy - A Major Partner of the Sustainable Development," *Mater. Sci. Forum*, vol. 455–456, no. 1, pp. 857–860, 2004.

[41] J. E. Foss and D. DeFranco, "The Northstar Cam Bearing Caps; A New Application for Aluminum P/M," in *SAE International Congress and Exposition*, 1994, p. Technical Paper No. 940429.

[42] D. P. Bishop, B. Hofmann, and K. R. Couchman, "Properties and Attributes of Commercially Available AC2014-Type Aluminum P/M Alloys," in *Advances in Powder*

Metallurgy and Particulate Materials, 1st ed., H. Ferguson and D. T. Whychell, Eds. Princeton, New Jersey: MPIF, 2000, pp. 87–100.

[43] A. D. P. LaDelpha, H. C. Neubing, and D. P. Bishop, "Metallurgical Assessment of a 7xxx Series PM Alloy," *Mater. Sci. Eng. A*, vol. 520, pp. 105–113, 2009.

[44] A. Ibrahim, D. P. Bishop, and G. J. Kipouros, "Sinterability and characterization of commercial aluminum powder metallurgy alloy Alumix 321," *Powder Technol.*, vol. 279, pp. 106–112, 2015, doi: 10.1016/j.powtec.2015.04.001.

[45] H. Asgharzadeh and A. Simchi, "Hot deformation of PM Al6061 alloy produced by sintering and powder extrusion," *Powder Metall.*, vol. 51, no. 4, pp. 354–360, 2008, doi: 10.1179/174329008X286695.

[46] H. Asgharzadeh, A. Simchi, and H. S. Kim, "Dynamic restoration and microstructural evolution during hot deformation of a P/M Al6063 alloy," *Mater. Sci. Eng. A*, vol. 542, pp. 56–63, 2012, doi: 10.1016/j.msea.2012.02.031.

[47] G. A. W. Sweet, B. W. Williams, A. Taylor, R. L. Hexemer, I. W. Donaldson, and D. P. Bishop, "A microstructural and mechanical property investigation of a hot upset forged 2xxx series aluminum powder metallurgy alloy reinforced with AlN," *J. Mater. Process. Technol.*, vol. 284, no. April, p. 116742, 2020, doi: 10.1016/j.jmatprotec.2020.116742.

[48] R. E. D. Mann, R. L. Hexemer, I. W. Donaldson, and D. P. Bishop, "Hot deformation of an Al-Cu-Mg powder metallurgy alloy," *Mater. Sci. Eng. A*, vol. 528, no. 16–17, pp. 5476–5483, 2011, doi: 10.1016/j.msea.2011.03.081.

[49] A. M. Ibrahim, D. P. Bishop, and G. J. Kipouros, "Effect of swaging and rolling post sintering treatments on the corrosion behaviour of Alumix 321 PM alloy," *Powder Technol.*, vol. 320, pp. 89–98, 2017, doi: 10.1016/j.powtec.2017.07.034.

[50] I. A. MacAskill, A. D. P. Ladepha, J. H. Milligan, J. J. Fulton, and D. P. Bishop, "Effects of cold and hot densification on the mechanical properties of a 7XXX series powder metallurgy alloy," *Powder Metall.*, vol. 52, no. 4, pp. 304–310, 2009, doi: 10.1179/174329009X409723.

[51] R. S. Kaneko, L. Bakow, and E. W. Lee, "Aluminum alloy 6013 sheet for new U.S. Navy

aircraft," *J. Miner. Met. Mater. Soc.*, vol. 42, no. May, pp. 16–18, 1990, doi: https://doi.org/10.1007/BF03220941.

[52] R. Braun, "Investigation on the long-term stability of 6013-T6 sheet," *Mater. Charact.*, vol. 56, no. 1, pp. 85–95, 2006, doi: 10.1016/j.matchar2005.03.006.

[53] MPIF, "Method for Determination of Apparent Density of Metal Powders Using the Arnold Meter," MPIF 48, 2019.

[54] MPIF, "Method For Determination Of Density Of Compacted Or Sintered Powder Metallurgy (PM) Products Materials," MPIF 42, 2019.

[55] MPIF, "Determination of Green Strength of Compacted Powder Metallurgy (PM) Materials," MPIF 15, 2019.

[56] Aluminum Association, *Aluminum Design Manual*. Arlington: Aluminum Association, 2020.

[57] MPIF, "Standard Test Methods for Tension Testing of Metallic Materials," MPIF E8-M, 2021.

[58] MPIF, "Determination of Rotating Beam Fatigue Properties of Powder Metallurgy (PM) Materials," MPIF 56, 2019.

[59] MPIF, *Determination of Transverse Rupture Strength of Powder Metallurgy (PM) Materials*. 2014.

[60] G. A. W. Sweet *et al.*, "Microstructural evolution of a forged 2XXX series aluminum powder metallurgy alloy," *Mater. Charact.*, vol. 151, no. February, pp. 342–350, 2019, doi: 10.1016/j.matchar.2019.03.033.

[61] I. A. MacAskill, R. L. Hexemer, I. W. Donaldson, and D. P. Bishop, "Effects of magnesium, tin and nitrogen on the sintering response of aluminum powder," *J. Mater. Process. Technol.*, vol. 210, no. 15, pp. 2252–2260, 2010, doi: 10.1016/j.jmatprotec.2010.08.018.

[62] M. J. Starink, "Analysis of aluminium based alloys by calorimetry: Quantitative analysis of reactions and reaction kinetics," *Int. Mater. Rev.*, vol. 49, no. 3–4, pp. 191–226, 2004,

doi: 10.1179/095066004225010532.

[63] Various, *ASM Handbook Volume 19: Fatigue and Fracture*. ASM International, 1996.